Review

Cu-Based Z-Schemes Family Photocatalysts for Solar H2 Production

Rossella Greco [1], Romain Botella [1] and Javier Fernández-Catalá [1,2,*]

[1] Nano and Molecular Systems Research Unit, University of Oulu, 90014 Oulu, Finland; rossella.greco@oulu.fi (R.G.); romain.botella@oulu.fi (R.B.)

[2] Materials Science Institute and Inorganic Chemistry Department, University of Alicante, Ap. 99, 03080 Alicante, Spain

* Correspondence: j.fernandezcatala@ua.es

Abstract: Solar photocatalytic H_2 production has drawn an increasing amount of attention from the scientific community, industry, and society due to its use of green solar energy and a photocatalyst (semiconductor material) to produce green H_2. Cu-based semiconductors are interesting as photocatalysts for H_2 production because Cu is earth-abundant, cheap, and the synthesis of its copper-containing semiconductors is straightforward. Moreover, Cu-based semiconductors absorb visible light and present an adequate redox potential to perform water splitting reaction. Nevertheless, pristine Cu-based semiconductors exhibit low photoactivity due to the rapid recombination of photo-induced electron-hole (e^--h^+) pairs and are subject to photo corrosion. To remedy these pitfalls, the Cu semiconductor-based Z-scheme family (Z-schemes and S-schemes) presents great interest due to the charge carrier mechanism involved. Due to the interest of Z-scheme photocatalysts in this issue, the basic concepts of the Z-scheme focusing on Cu-based semiconductors are addressed to obtain novel systems with high H_2 photo-catalytic activity. Focusing on H_2 production using Cu-based Z-schemes photocatalyst, the most representative examples are included in the main text. To conclude, an outlook on the future challenges of this topic is addressed.

Keywords: copper; H_2 production; photocatalysis; semiconductors; Z-scheme family
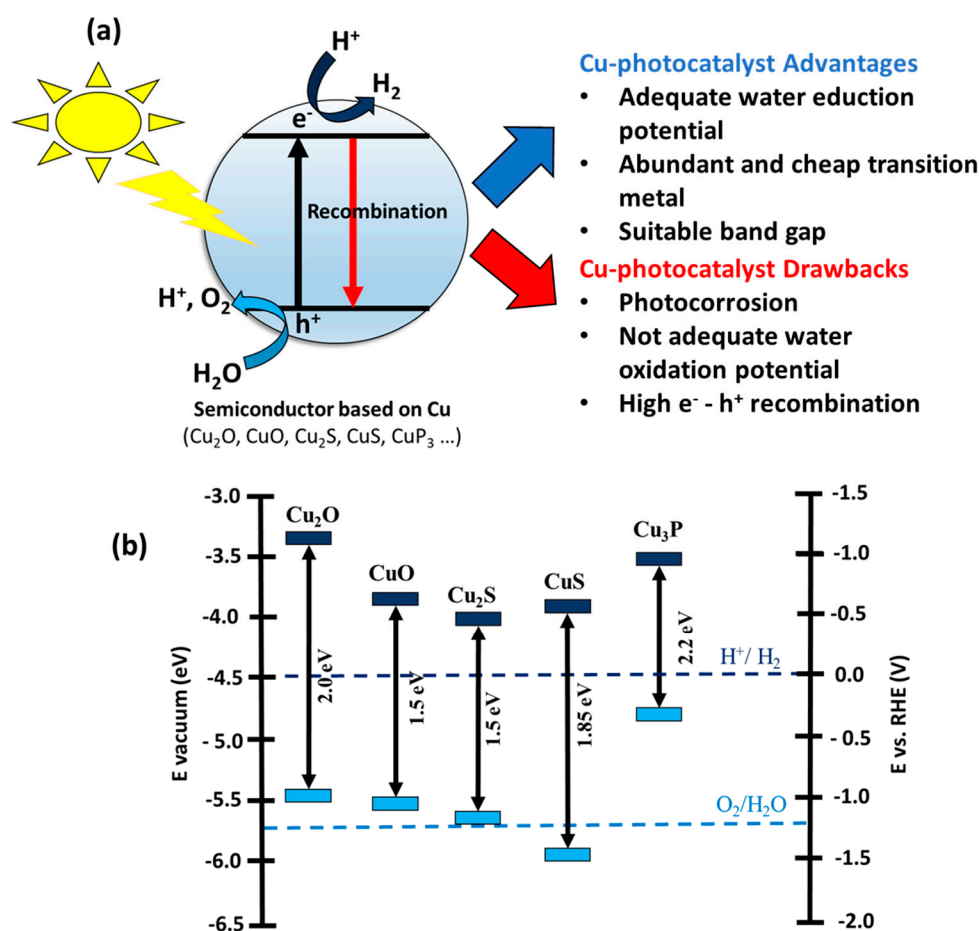
1. Introduction

Some of the great challenges nowadays in our society are energy production and environmental protection since they have a large negative impact on our society, affecting, among others, air quality, climate, and economy [1,2]. Such problems have been caused by rapid industrialization, uncontrolled environmental pollution, and the current energy scenario based on fossil fuels. This fact needs the development and increase in the use of renewable energies to ensure independence from "fossil fuels" to prevent further environmental degradation [3]. With this scenario, hydrogen (H_2) is considered an ideal solution for changing the current fossil fuel-based technology to a green technology due to the fact that H_2 possesses a high energy density without generating CO_2 emissions [4,5]. Moreover, H is the most abundant element on earth. However, hydrogen in nature is found in combination with other elements (oxygen in water and carbon in natural gas) [6]. Currently, H_2 is mainly produced by non-renewable sources such as steam methane reforming, coal gasification, and coal pyrolysis [7]. To implement the H_2 economy in our society, the development of new technologies is essential to allow the production of H_2 without using fossil fuels [4]. Consequently, the generation of H_2 by water splitting has attracted the attention of the scientific community and society because this reaction does not produce CO_2 [8,9]. However, the water-splitting reaction (Equation (1)) is a non-spontaneous endergonic reaction (ΔG = +237 KJmol^{-1}), which means that energy is needed for the reaction to occur [10]:

$$H_2O \rightarrow \text{\textonehalf}O_2 + H_2 \left(\Delta G = 237 \text{ KJmol}^{-1} \right) \qquad (1)$$

As we can notice from Equation (1), another key point in the water splitting reaction is the generation of oxygen as a sub-product of the reaction, making necessary the purification of the H_2 [11,12].

One alternative to producing H_2 from water splitting using renewable energy is photocatalysis, which requires the use of sunlight and a semiconductor [9,13]. The photocatalytic mechanism, see Figure 1a, might be described briefly as follows: Initially, a photon with energy equal to or greater than the energy band gap (Eg) of the semiconductor is absorbed by the semiconductor. This phenomenon promotes a (photo-excited) electron from the valence band (VB) to the conduction band (CB), generating an electron–hole pair (e^--h^+). The produced e^- and h^+ can migrate to the surface of the semiconductor and initiate the redox reaction(s) with H_2O or H^+ to produce O_2 and H_2; nevertheless, the e^--h^+ pair can recombine and hinder the photo-catalytic activity [14,15]. Photo-catalysis technology has been receiving an increased amount of attention for its use in H_2 production after the pioneering work reported by Fujishima and Honda in 1972 based on photoelectrochemical water splitting on a TiO_2 electrode [16]. In this work, the authors showed that it is possible to perform water splitting reaction using TiO_2 as a semiconductor and UV light as an energy source. However, TiO_2 is not active under solar light due to its high band gap (3.1 eV). Additionally, the pristine TiO_2 presents a high e^--h^+ recombination ratio, which is one of the main drawbacks of the use of TiO_2 as a photocatalyst [17,18].

Figure 1. (**a**) Scheme of photo-catalysis on a Cu-based semiconductor and the advantages and drawbacks of its use in H_2 production. (**b**) Energy band diagram of several Cu-based semiconductors.

With this in mind, the scientific community has been focused on developing photocatalysts that can use solar light to efficiently and more environmentally friendly produce H_2 instead of using semiconductors with a high band gap [13,19]. Moreover, semiconductors based on earth-abundant and inexpensive metals (Cu, Ni, Fe, etc.) have been developed

due to their interesting potential as viable alternatives to rare and expensive noble metal photocatalysts [20,21]. One family of transition-metal semiconductors that is gaining the attention of the scientific community for application in photo-catalysis is the one based on copper "Cu-based semiconductors" such as Cu_xO and Cu_xS, among others [22,23]. Cu-based semiconductors are attractive for their use as photocatalysts because copper is abundant on earth, presents a low cost, and its synthesis is straightforward [24]. Regarding the application of Cu-based semiconductor materials in photo-catalytic H_2 production, they are promising materials due to their tunable band gaps, band alignment with respect to the water reduction potential (Figure 1b), and easy synthetic process, with respect to other semiconductors based on transition metals such as Ni, Fe, or Co [22,25–29]. In this sense, Cu-based oxide/chalcogenide semiconductors present a higher reduction potential than H^+/H_2 redox potential, indicating that these semiconductors may be active for water splitting [30]. Moreover, Cu-based semiconductors are active under visible light because they have a low band gap between 1.5 eV and 2.2 eV [31]. However, pristine Cu-based semiconductor materials exhibit low photoactivity in H_2 production due to the rapid recombination of photo-induced e^--h+ pairs [32]. Also, another important drawback of this family of semiconductors is that the oxidation potential of some materials, such as Cu_2O, CuO, and Cu_3P, is not suitable to perform the overall water splitting reaction [21]. However, the most important drawback of Cu-based semiconductor materials for their possible commercialization is the low stability of these materials under reaction conditions due to photo-corrosion [33,34]. This is caused by the ability of copper to be both reduced ($Cu^{+I} + e^- \rightarrow Cu^0$) and oxidized ($Cu^{+I} + h^+ \rightarrow Cu^{+II}$) by photogenerated e^- and h^+, respectively [22]. To improve the photo-catalytic efficiency of Cu-based semiconductor materials in H_2 production, several strategies have been developed by the scientific community [34], i.e., doping elements [35], deposition of metals [36], and construction of heterojunctions [37,38]. In this sense, the use of metal and co-catalysts to boost the catalytic activity of the semiconductor has been widely studied by the scientific community [39,40].

One alternative to obtain effective separation of photogenerated e^--h^+ pairs, avoid the photocorrosoin of Cu-based semiconductors, and improve their catalytic activity is mimicking the natural photosynthetic systems (Z-Scheme charge transfer), where H_2O is cleaved into O_2 and the H_2 equivalent species by a double excitation mechanism [41]. In this sense, the two half-reactions are spatially separated in photosystem I (PSI) and photosystem II (PS II), starting a 'Z-scheme' charge transfer mechanism (see Figure 2a) [42]. Inspired by natural photosynthesis, in the last years, the scientific community is focused on developing materials like semiconductors to construct the Z-scheme heterojunctions family (Z-Scheme and S-scheme), see Figure 2b, consisting of an H_2 evolution photocatalyst and an O_2 evolution photocatalyst for efficient water splitting [43,44]. Indeed, the Z-scheme family systems present accessibility to photoexcited carriers with greater redox potential, separation of oxidative and reductive hubs, mediator-free charge transfer between the semiconductors, and enhanced light absorption ability [45].
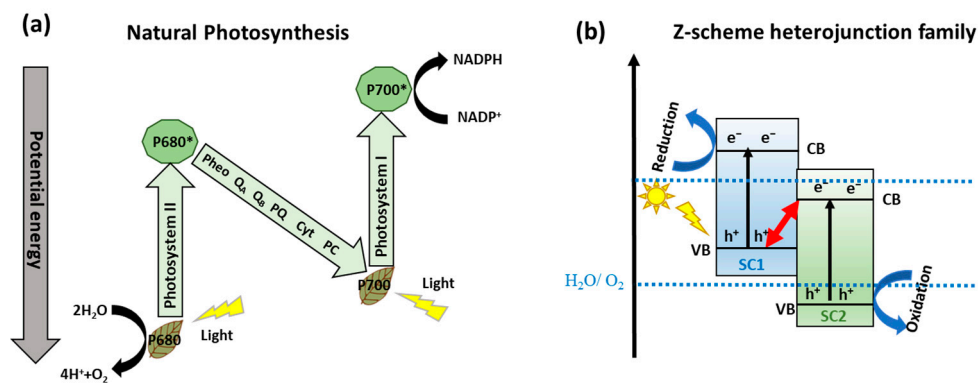
Figure 2. (**a**) Scheme of natural photosynthesis mechanism process. Reproduced from [38]. (**b**) Z-scheme schematic diagram for two semiconductors. Adapted from [46].

Z-schemes family heterojunctions (Z-schemes and S-schemes) using several semi-conductors such as TiO_2, $BiVO_4$, etc., are applied in relevant photo-catalytic reactions, i.e., environmental applications, energetic applications, transformation of organic compounds into high added-value products, and photo-catalytic biorefineries [47,48]. This review will describe in depth the Z-Schemes family based on Cu due to the relevance of these abundant and cheap metal-based photocatalysts. The mini-review will cover the most relevant works on Cu-based Z-scheme photocatalysts for their use in energy aspects, focusing on a relevant application such as H_2 production. This novel technology based on a low transition metal (Cu) has received the attention of the scientific community, increasing the number of publications about this topic during the last few years.
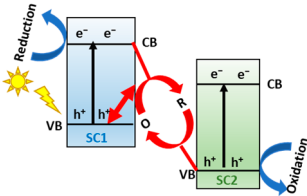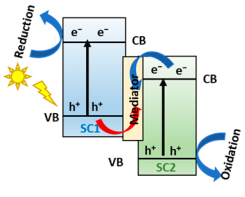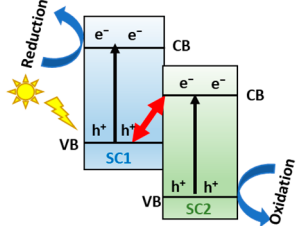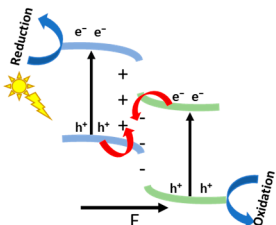
2. Z-Schemes Family Based on Cu

Semiconductor-based photocatalysis technology is still limited for commercialization by its low quantum yield, low utilization rate of visible light, and high recombination rate of photogenerated e^--h^+ pairs [49,50], as mentioned in the Introduction section. In order to improve the photo-catalytic efficiency of semiconductors, several aspects should be taken into account, such as charge separation and absorption in visible light [13,46]. Cu-based semiconductors are promising photocatalysts, considering their low band gap between 1.5 eV and 2.2 eV and consequent absorption of visible light [31], but they present a high e^--h^+ pairs recombination rate and photo corrosion [32,34] (see Introduction section).

One alternative to solve these drawbacks is to develop heterojunction systems [51,52], which are defined as the 'junction' of different semiconductors in intimate contact [44]. The heterojunction photocatalysts can be classified into different categories [53]. Considering the band alignment between the CBs and VBs of the semiconductors composing the heterojunction, this can be classified into three types [54] (see Table 1):

Table 1. Summary of different types of heterojunctions.

Photo-Catalytic System	Advantages	Drawbacks	Representation of Mechanism
Type I	-	Fast recombination	
Type II	Improve charge separation efficiency	Low oxidation and reduction potential	
Type III	-	Not synergistic effect between semiconductors	

Table 1. *Cont.*

Photo-Catalytic System	Advantages	Drawbacks	Representation of Mechanism
Liquid-phase Z-scheme	Higher redox ability than traditional heterojunction	The reaction is performed in liquid phase. Difficult application	
All-solid-state Z-scheme	Strong redox ability in solid state	High cost of noble metals	
Direct Z-scheme	Strong redox ability without the use of mediators	The mechanism is controversial	
S-scheme	Controllable built-in electric field intensity and stable interfacial carrier transport process, Strong redox ability, and clear mechanism.	Mainly n-type semiconductors	

(I) Straddling-gap junctions (Type I): In this junction, the semiconductor I (SI) has a higher CB and a lower VB than the semiconductor II (SII). So, the e^- and h^+ move to the CB and VB from SI to SII. Then, the charge carriers are not properly separated due to their aggregation on the same semiconductor, favoring the recombination.

(II) Staggered-gap junctions (Type II): In this junction, the semiconductor I (SI) has a higher CB and VB than the semiconductor II (SII). Then, e^- and h^+ will move to their corresponding low-energy bands. As a result, the photo-catalytic efficiency of the systems will be improved due to the charge carriers' separation; nevertheless, the redox capacities will be reduced since the e^- and h^+ are in the bands with low energy potentials.

(III) Broken-gap junctions (Type III): The band gaps do not overlap at all. e^- and h^+ stay in their original semiconductors without charge migration, so the two semiconductors work separately without any synergistic effect.

As was mentioned in the classification, Type II junctions present a great interest in photo-catalytic H_2 production due to the charge carriers' separation, one of the main problems of using Cu-based semiconductors [55]. However, these materials might be useless for this application due to the diminished redox capacity of these materials [56,57]. To solve this challenge, the scientific community has been focusing on exploring novel junction types, namely the Z-scheme system. These heterojunctions aim to mimic the photosynthetic process [41,56]. Both Z-scheme and Type II heterojunctions present the same staggered band alignment, but the charge transfer is different. In Z-schemes, e^- of SI are recombined with h^+ of SII, allowing a stronger redox ability of the Z-scheme heterojunctions compared to the Type II heterojunctions. So, the development of emerging

Z-scheme heterojunctions based on Cu is very meaningful and important for achieving high-efficiency photo-catalytic reactions [45,58]. Proposed for the first time by Bard in 1979 [59], this system needs a shuttle redox mediator (electron acceptor/donor pair) to form a liquid-phase Z-scheme (traditional Z-scheme), but its main limitation is the redox mediator reversibility because they can only be applied in the liquid phase [44,60]. In 2006, Tada et al. proposed all-solid-state Z-scheme photocatalysts (second-generation Z-scheme) [61]. These systems are composed of two different semiconductors with a solid-phase electron mediator as noble metal nanoparticles or carbon material (graphene and carbon nanotubes) [62]. The noble metals used as a mediator present a limitation for the efficiency and applicability of the process because they are rare and expensive [56]. In addition, mediators used in the all-solid-state Z-scheme can produce the Schottky junction, restricting the continuous flow of electrons by the Schottky circuit [63]. In 2013, Yu et al. [64] constructed a direct Z-scheme photocatalyst (third-generation Z-Scheme) combining g-C_3N_4 and TiO_2 to solve the inconvenience of using an electron mediator since the interfacial contact between the semiconductors facilitates the direct electron transfer [43]. The main limitation of direct Z-schemes is that the overall concentration of photocarriers in direct Z-scheme photo-catalytic materials is reduced by the charge carriers' recombination at the interface, resulting in a lower quantum yield of the photocatalyst [44].

To address the above problems of type-II heterojunction, traditional Z-scheme, and all-solid-state Z-scheme systems, with the difficulty of demonstrating the direct Z-scheme mechanism charge transfer, a new step-scheme (S-scheme) heterojunction concept was proposed based on direct Z-scheme heterojunction [44,65]. Then, the development of S-scheme heterojunctions is a historical necessity to describe adequately the charge transfer in direct Z-scheme systems [66]. In the S-scheme [44], a reductant photocatalyst (RP) and oxidant photocatalyst (OP) come into contact; hence, e^- in RP with a higher Fermi level will drift to the OP with a lower Fermi level at the interface. In other words, the RP side loses e^- and is positively charged. Contrarily, the OP side accepts e^- and becomes negatively charged. Additionally, upward or downward band bending occurs at the interface of RP and OP, respectively. Concurrently, a built-in electric field whose direction points from RP to OP is formed. Under light irradiation, said electric field drives the photogenerated e^- transferring them from CB of OP to VB of RP. Moreover, the Coulombic attraction between e^- in OP and h^+ in RP and band bending also favors this charge transfer. On the contrary, Coulombic repulsion, band bending, and a built-in electric field also inhibit the electron transfer from CB of RP to CB of OP and the hole transfer from VB of OP to VB of RP. Ultimately, the powerful photogenerated e^- and h^+ are reserved in the CB of RP and VB of OP, respectively. Therefore, strong redox ability is earned in the S-scheme photocatalyst. The S-scheme heterojunction system collectively achieves charge separation and exhibits strong photo-redox ability, which results in improved photo-catalytic performance [44].

With this in mind, in this review, we will focus on the scientific works based on all-solid-state Z-scheme, direct Z-scheme, and S-scheme due to the advantages described in this section and their promising future applications. Moreover, this review will be focused on the use of Cu-based semiconductors as a part of Z-scheme photocatalysts. This fact is due to the interesting properties of Cu-based semiconductors in terms of visible light adsorption and suitable redox potentials previously described in the Introduction section to obtain photocatalysts with high activity in photo-catalytic H_2 production.

3. H_2 Production by Z-Schemes Based on Cu

As mentioned in the previous sections, Cu-based direct Z-schemes have been widely studied by scientists for their application in photo-catalytic H_2 production due to the great properties of these systems, such as adequate charge transfer and high redox ability [24]. In this section, the most representative Cu-based Z-schemes (all-solid-state Z-scheme, direct-Z-scheme, and S-scheme) and their use in H_2 production will be presented. Additionally, in the main text, the most relevant aspects of the developed direct Z-schemes based on copper are also described.

3.1. Cu Oxides-Based Z-Schemes (Family)

Cu-based metal oxides, such as Cu_2O and CuO, are among the most studied metal oxides owing to their non-toxicity, availability in nature, and suitable band gaps. Due to their unique optoelectronic properties, they have been extensively used in energy conversion, storage, and sensing devices [30,67].

Cu_2O is a p-semiconductor with a band gap in the visible range (2.2 eV). This characteristic makes it very interesting for photo-catalytic applications, but like many narrow band gap semiconductors, it suffers from poor photostability [33]. For this reason, many heterostructures have been successfully studied in the literature, and some of the Z-schemes family heterojunctions are resumed in Table 2.

Among others, TiO_2 has been extensively applied as a component in heterojunctions for photo-catalytic applications in order to overcome its biggest drawback, i.e., its wide band gap (>3 eV), which brings to inactivity in the visible range [68]. Wei et al. demonstrated that even different facets of TiO_2 are relevant in the stabilization of Cu_2O. Indeed, a Cu_2O/TiO_2 Z-scheme heterostructure with exposed 101-faceted TiO_2 facets and oxygen vacancies exhibited extremely higher activity for solar water splitting and unpredicted photostability compared to a 001-faceted TiO_2 Type II Cu_2O/TiO_2 junction, as shown in Figure 3a. A DFT-based density of states (DOS) was used to explain the impact of defects on the electronic structures, namely the appearance of gap states coming from Ti-located dangling bonds [69]. The improved photocatalytic activity obtained using Cu_2O/TiO_2 was confirmed by Lv et al. In this case, not only could the mesoporous TiO_2 increase the photostability of Cu_2O in a Z-scheme, but also provide more active sites due to its high surface area [70]. Furthermore, in the work of Fu et al., the presence of Ag as an electron mediator enhanced the visible light absorption and the photo-catalytic activity by forming a dual Z-scheme $TiO_2/Ag/Cu_2O$ [71]. Interestingly, the Cu_2O/TiO_2 showed promising activity even in the form of film stripes. Zhu et al. distributed Cu_2O and TiO_2 in parallel on fluorine-doped tin oxide (FTO) to obtain a film photocatalyst as opposed to the more conventional particulate materials. The result was an active photocatalyst for overall water splitting, and it gave insights into the design of Z-scheme photocatalysts [72].

As TiO_2, ZnO can be listed as one of the most used photocatalysts, but it presents the same disadvantage, i.e., a wide band gap of 3.37 eV [73]. Heterostructures composed of Cu_2O and ZnO will be endowed with the positive sides of both components, such as absorption in the visible range and low photo corrosion, respectively. Indeed, the S-scheme Cu_2O/ZnO showed less recombination than the pure components, which was reflected in a higher catalytic activity of the composite [74]. Moreover, in the Z-scheme ZnO/Cu_2O-CuO, the CuO could improve the photocatalytic performance of the composite made only by ZnO and Cu_2O (see Figure 3b) [75].

Carbon-based materials are ideal components in heterojunctions, considering that carbon is one of the most abundant elements on Earth. Thus, $g-C_3N_4$ has been widely used as a photocatalyst due to its absorption in the visible range and potential activity in H_2 evolution and pollutant degradation [46]. Unfortunately, it suffers from a high recombination rate and synthetic difficulties, which result in too low activity. To solve these issues, different heterojunctions have been studied, and Cu_2O has also been used as part of them to overcome the drawbacks of both materials. Xu et al. synthesized a high surface area $Cu_2O/g-C_3N_4$ Z-scheme, where the $g-C_3N_4$ benefitted the presence of Cu^{2+} ions for an easier synthesis, to obtain a highly active photocatalyst for H_2 evolution (see Figure 3c) [76]. While in the previous work, Cu_2O nanoparticles resulted in a $Cu_2O/g-C_3N_4$ Z-Scheme, Dai et al. could prepare an S-scheme using Cu_2O octahedrons. The obtained $Cu_2O/g-C_3N_4$ S-scheme demonstrated high activity in H_2 production but also in the reduction of Cr^{6+} and oxidation of tetracycline. Charge transfer was illustrated with charge density profiles obtained computationally [77]. Similar Cu_2O octahedrons were used in the all-solid Z-scheme $Cu(OH)_2/Cu_2O/g-C_3N_4$, where the presence of Cu as an electron mediator and of $Cu(OH)_2$ as a semiconductor could increase the activity towards H_2 compared to the pure compounds composing the heterojunction [78]. The performance of heterojunctions

in photo-catalytic H_2 production can also be improved by adding new sites in the form of doping or decoration. In these cases, it is worth mentioning the works of Gu et al. and Mu et al. The former could prove an increased light stability of Cu_2O by doping it with sulfur in the Z-scheme Cu_2O/g-C_3N_4 [79]. Additionally, the plasmonic effect obtained by decorating with Au nanoparticles could increase the photo-catalytic H_2 evolution and the interfacial charge separation in the S-scheme Au/g-C_3N_4/Cu_2O [80].

Different studies have been made on Cu_2O composites, and the Z-schemes RGO-Cu_2O/Fe_2O_3 and RGO-Cu_2O/Bi_2WO_6, where RGO acts as a mediator, represent good examples of the potential of Cu_2O in photo-catalysis [81,82]. Both heterojunctions were proven to have improved activity and could benefit from the advantages of each component, even without the use of sacrificial agents.

Among copper oxides, CuO definitely has a pivotal role in catalysis and photo-catalysis. It is a p-semiconductor whose band gap ranges from 1.2 eV to 2.0 eV, making it active in visible light [83]. As mentioned above, narrow band gap materials frequently possess a common drawback, i.e., a high recombination rate. On the other hand, these kinds of materials are absorbed in the visible range, arousing the interest of their application in visible light-mediated processes. Hence, CuO has also been used in several Z-scheme family heterojunctions. Even though CuO nanostructures do not always have the correct potential energy for hydrogen evolution, CuO-based heterojunctions are demonstrated to profit from the presence of this material [84]. Chu et al. described a successful Z-scheme formed by CuO and polyimide (PI) for H_2 production. In this case, the presence of CuO decreased the well-known inadequate space charge separation of polymers [85]. In the S-schemes g-$C_3N_4/TiO_2/CuO$ and $CuO/CdS/CoWO_4$, the improvement in the catalytic activity was demonstrated to be related to the close interface contact in the double heterojunction. The second could avoid all the disadvantages related to the single components, i.e., recombination rate (g-C_3N_4, CdS, CuO), photo corrosion (CdS), or wide band gap (TiO_2) [86,87]. Ahmad et al. proved the importance of the surface plasmon resonance (SPR) effect caused by Au in the S-scheme $ZnO/CuO/Au$. Indeed, the SPR was considered one of the reasons for the increased photocatalytic activity in H_2 production [88]. The combination of both Cu oxides and ZnO brought to the extremely active Z-scheme $ZnO/CuO/Cu/Cu_2O/TiO_2$, where the use of Cu could improve the light absorption of TiO_2 [89]. Finally, Kannan et al. showed how the presence of the multilayered 2D structure, Ti_3AlC_2, improved the activity of the CuO/NiO composite. The extremely active S-scheme $Ti_3AlC_2/CuO/NiO$ was prepared, and it was demonstrated to possess a very long charge carrier lifetime (3 ns), as shown in Figure 3d [90].

Up to now, only binary compounds were considered, but the synergistic effect in ternary and quaternary transition metals-based photocatalysts is recently becoming of central relevance due to their more tunable band gaps and decreased photocorrosion compared to the monometallic counterparts. $CuFeO_2$ or delafossite is a promising mixed oxide with a narrow band gap (1.30 eV), and it was demonstrated to be active in H_2 production in the Z-scheme with $Bi_{20}TiO_{32}$ [91]. On the other hand, $CuBi_2O_4$ is a suitable photocatalyst for visible light-mediated processes due to its band gap of 1.5–1.8 eV, but it shows fast recombination. Hence, Mao et al. demonstrated that the construction of the S-scheme $CuBi_2O_4/Na$-TiO_2 could decrease the recombination in $CuBi_2O_4$ and increase the visible light absorption of TiO_2 [92].

Finally, polyoxometalates can be mentioned in the family of mixed oxides, considering that they are formed by a metal anion composed of Mo or W and O and a metal cation, in our case, copper. Indeed, these compounds are extremely interesting for energy applications due to their semiconducting properties and the possibility of easily tuning their structure [93]. $CuWO_4$ has been demonstrated to be applicable in catalysis, but also in photocatalysis to form Z-schemes with TiO_2 and allow high H_2 production in visible light-mediated processes [94,95]. Similarly, copper molybdates have shown great applicability in photocatalysis, and Li et al. demonstrated the decreased recombination of γ-graphyne (γ-GY) in the S-scheme $CuMoO_4/\gamma$-GY. In this work, the electronic structure of the het-

erojunction has been calculated through ab initio calculations; DOS was used to confirm the direction of the charge transfer and give some precision on the location of the e^-/h^+ migration [96].
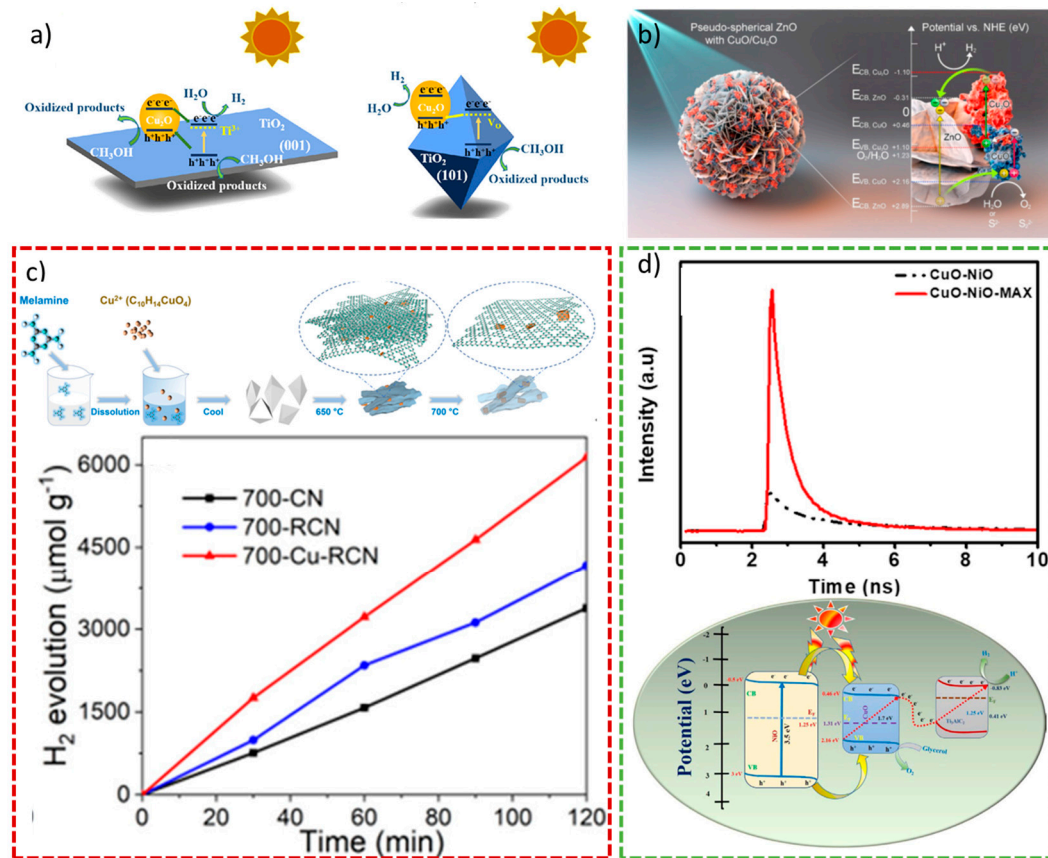
Figure 3. (**a**) Schematic diagrams of interfacial charge transfer in defective Cu_2O/TiO_2 Type II (**left**) and Cu_2O/TiO_2 Z-scheme (**right**) heterojunctions. Reproduced from [69]. Copyright 2019, ACS Publications. (**b**) Schematic illustration of the Z-scheme-assisted ZnO/Cu_2O-CuO heterojunction. Reproduced from [75]. Copyright 2020, Elsevier. (**c**) Synthetic process (**top**) and H_2 production (**bottom**) of Cu_2O/g-C_3N_4. Reproduced from [76]. Copyright 2022, ACS Publications. (**d**) Time-resolved photoluminescence spectrum (**top**) and plausible photocatalytic mechanism of $Ti_3AlC_2/CuO/NiO$ (**bottom**). Reproduced from [90]. Copyright 2023, Elsevier.

Table 2. Cu oxides-based Z-schemes family heterojunctions for H_2 production (AQE: apparent quantum efficiency; SA: sacrificial agent; NA: not available).

Photocatalyst	Fabrication Methodology	Irradiation Source	H_2 Production Activity and AQE	Reference
Cu_2O/TiO_2	Photodeposition	Xe lamp (300 W)	32.6 mmol g^{-1} h^{-1} AQE: 53.5% (350 nm) SA	[69]
Cu_2O/TiO_2	Adsorption-reduction	Xe lamp	11 mmol g^{-1} h^{-1} AQE: 15.1% (365 nm) SA	[70]
$TiO_2/Ag/Cu_2O$	Impregnation-calcination/ Photodeposition	Xe lamp (300 W)	874.7 μmol g^{-1} h^{-1} AQE: 2.3% (365 nm) SA	[71]

Table 2. *Cont.*

Photocatalyst	Fabrication Methodology	Irradiation Source	H$_2$ Production Activity and AQE	Reference
TiO$_2$/FTO/Cu$_2$O	Impregnation-calcination/ Electrodeposition	Xe lamp (300 W)	200 µmol m^{-2} AQE: NA SA	[72]
Cu$_2$O/ZnO	Impregnation	Xe lamp (150 W)	208.9 µmol g^{-1} h^{-1} AQE: 8.8% (500 nm) SA	[74]
ZnO/Cu$_2$O-CuO	Thermal oxidation	Xe lamp (150 W)	1.1 mmol g^{-1} h^{-1} AQE: 3.0% SA	[75]
Cu$_2$O/g-C$_3$N$_4$	Recrystallization– calcination	Xe lamp (300 W, λ ≥ 420 nm)	5.8 mmol g^{-1} h^{-1} AQE: 13.4% SA	[76]
Cu$_2$O/g-C$_3$N$_4$	Impregnation	Xe lamp (500 W, λ ≥ 400 nm)	480.6 µmol g^{-1} h^{-1} AQE: NA SA	[77]
Cu(OH)$_2$/Cu$_2$O/g-C$_3$N$_4$	Sonoprecipitation/ Impregnation	Metal halide lamp (150 W, UV cut-off)	622.0 µmol g^{-1} h^{-1} AQE: NA SA	[78]
S-Cu$_2$O/g-C$_3$N$_4$	Sonication	Xe lamp (300 W, λ ≥ 420 nm)	620.7 µmol g^{-1} h^{-1} AQE: NA SA	[79]
Au/g-C$_3$N$_4$/Cu$_2$O	Impregnation	Xe lamp (500 W, λ ≥ 400 nm)	552.6 µmol g^{-1} h^{-1} AQE: NA SA	[80]
RGO-Cu$_2$O/Fe$_2$O$_3$	Hydrothermal	Xe lamp (300 W, λ ≥ 420 nm)	4.86 µmol g^{-1} h^{-1} AQE: NA	[81]
RGO-Cu$_2$O/Bi$_2$WO$_6$	Solvothermal	Xe lamp (300 W, λ ≥ 420 nm)	1.80 µmol g^{-1} h^{-1} AQE: NA	[82]
CuO/PI	Solvothermal	Xe lamp (300 W, λ ≥ 420 nm)	104.6 µmol g^{-1} h^{-1} AQE: 5.8% (450 nm) SA	[83]
g-C$_3$N$_4$/TiO$_2$/CuO	Impregnation	Xe lamp (300 W)	97.5 µmol g^{-1} h^{-1} AQE: NA SA	[84]
CuO/CdS/CoWO$_4$	Microwave	Xe lamp (300 W, λ ≥ 420 nm)	457.9 µmol g^{-1} h^{-1} AQE: NA SA	[87]
ZnO/CuO/Au	Sol–gel	Xe lamp (300 W, λ ≥ 400 nm)	4.7 mmol g^{-1} h^{-1} AQE: NA SA	[88]
Ti$_3$AlC$_2$/CuO/NiO	Sonication– Calcination	Solar simulator	20.7 mmol g^{-1} h^{-1} AQE: 14.2% (365 nm) SA	[90]
IrO$_2$/Bi$_{20}$TiO$_{32}$/CuFeO$_2$/rGO	Impregnation	Xe lamp (500 W)	1.1 mmol g^{-1} h^{-1} AQE: 4.8%	[91]
CuBi$_2$O$_4$/Na-TiO$_2$	Hydrothermal	Xe lamp (300 W)	2.7 mmol g^{-1} h^{-1} AQE: NA SA	[92]

Table 2. *Cont.*

Photocatalyst	Fabrication Methodology	Irradiation Source	H$_2$ Production Activity and AQE	Reference
CuWO$_4$/TiO$_2$	Impregnation	Solar simulator	106.7 mmol g^{-1} h^{-1} AQE: NA SA	[94]
CuWO$_4$/TiO$_2$	Hydrothermal	Hg lamp (500 W)	9.85 mmol g^{-1} h^{-1} AQE: NA SA	[95]
CuMO$_4$/γ-GY	Hot solvent	NA	4 mmol g^{-1} h^{-1} AQE: NA SA	[96]

3.2. Cu Sulfides-Based Z-Schemes (Family)

Cu-based sulfides are promising semiconducting materials for several applications, including photovoltaics, photo-electrocatalysis, energy storage, energy conversion, sensing, CO$_2$ reduction, and organic degradation [97,98]. Some Z-scheme family heterojunctions composed of Cu sulfides are resumed in Table 3.

Among all the copper sulfides, Cu$_2$S has been studied as a component of Z-scheme family heterojunctions for its positive properties, such as a narrow band gap (2.2 eV) [25]. Ranjith et al. discovered that Cu$_2$S could extend the visible light absorbance range, promote effective charge carrier separation in the Z-scheme ZnO/ZnS/Cu$_2$S, and improve H$_2$ production [99]. ZnCdS compounds have also been used as components in Cu$_2$S-based heterojunctions due to their tunable band gap and favorable photo-catalytic activity. Indeed, the S-scheme Cu$_2$S/ZnCdS and the Z-scheme Cu$_2$S/Zn$_{0.67}$C$_{0.33}$dS (see Figure 4a) reached quite excellent H$_2$ production, confirming these materials as extremely promising for energy applications [100,101].

Additionally, CuS has attracted a lot of interest and has been extensively used in photo-catalysis for its narrow band gap (from 1.88 eV to 2.16 eV), which is easily modifiable by changing the morphology of the material [102]. For this reason, it has been used in several heterojunctions to make the most of its properties and decrease its recombination rate. Kumar et al. demonstrated that in the Z-scheme CuS/Ag$_2$O/g-C$_3$N$_4$, CuS could provide not only an effective heterojunction interface but also more contacting sites to facilitate the formation of h$^+$ [103]. In the case of the Z-scheme CuS/CdS, both components presented a decreased recombination rate and intimately contacted interfaces (see Figure 4b) to improve the photo-catalytic H$_2$ production [104]. CuS was also successfully introduced by Liu et al. in an S-scheme with NiCo$_2$O$_4$ to improve the charge carriers' separation and transfer [105].

Cu$_7$S$_4$ is also finding its place in Z-schemes construction due to its narrow band gap [106]. Yuan et al. found two main advantages in the use of Cu$_7$S$_4$, i.e., the relevance of the Cu vacancies for the formation of the Z-scheme Cu$_7$S$_4$/MnS and the SPR effect to improve light harvesting [107]. Additionally, Cu$_7$S$_4$ could decrease the photo corrosion of CdS in the Z-scheme Cu$_7$S$_4$/CdS, thus improving the photocatalytic activity by enhancing the charge carrier's separation (see Figure 4c) [108].

In the following part, we analyze some of the ternary and quaternary sulfides used in Z-scheme family photocatalysts, which present improved characteristics compared to the monometallic compounds, as commented above. Among them, CuInS$_2$ represents the most studied and applied due to its light absorption in the visible range and suitable conduction band for H$_2$ evolution [109]. CuInS$_2$ has been used to improve the photocatalytic activity of g-C$_3$N$_4$ and take advantage of its more abundant active sites to form Z-schemes [110]. The use of noble metal nanoparticles has been demonstrated to improve the photocatalytic activity of the composite CuInS$_2$/g-C$_3$N$_4$ in the Z-scheme Au/CuInS$_2$/NCN-CN$_x$, as shown in Figure 4d. DFT calculations have been performed and were shallowly used as support for experimental results [111]. Zhong et al. reported the synthesis of the Z-

scheme Pt-CuInS$_2$/CdS with high photocatalytic activity, which was attributed to the photoinduced electron transfer from the defect-mediated trap states in CuInS$_2$ [112]. Yang et al. used CuInS$_2$ to successfully improve the absorption range of Ti$_3$C$_2$/TiO$_2$ to obtain an S-scheme with improved photocatalytic activity [113]. Finally, combining CuInS$_2$ with another bimetallic sulfide (Cd$_{0.5}$Zn$_{0.5}$S), an efficient S-scheme could be prepared with a large interfacial contact area, enhanced light absorption, and directional charge transfer and separation [114].

As in the case of ternary compounds, Cu-based quaternary sulfides have been extensively applied in Z-scheme photocatalysts. (CuGa)$_{1-x}$Zn$_{2x}$S$_2$ is one of the best examples, especially for overall water splitting in combination with semiconductors possessing the right potential to produce O$_2$ [115,116]. Additionally, Cu$_2$NiSnS$_4$ and Cu$_2$ZnSnS$_4$ have demonstrated the versatility of quaternary compounds in the preparation of Z-schemes. Indeed, they were shown to be active in H$_2$ production due to their higher stability and broader absorption spectra [117,118].
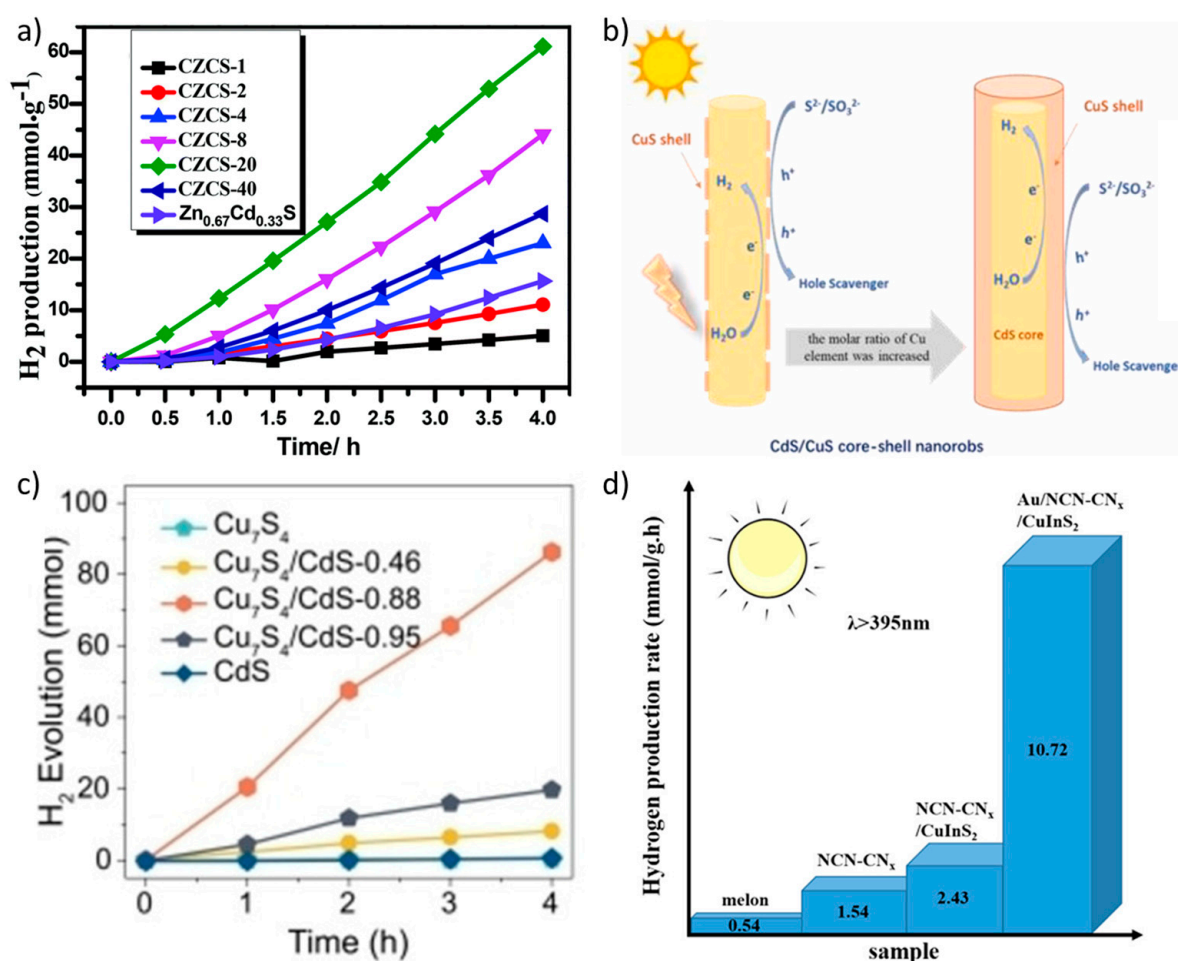
Figure 4. (**a**) Photocatalytic H$_2$ production of the Cu$_2$S/Zn$_{0.67}$C$_{0.33}$dS photocatalysts. Reproduced from [101]. Copyright 2019, RSC Publications. (**b**) Schematic illustration of CdS/CuS core-shell nanorods with different molar ratios of Cu element. Reproduced from [104]. Copyright 2023, Elsevier. (**c**) Photocatalytic H$_2$ production of CdS/Cu$_7$S$_4$ heterojunctions with different Cd content under visible-light irradiation. Reproduced from [108]. Copyright 2022, Wiley. (**d**) Comparison of H$_2$ production rates of g-C$_3$N$_4$, NCN-CNx, CuInS$_2$/NCN-CNx, and AuNPs/CuInS$_2$/NCNCNx. Reproduced from [111]. Copyright 2021, ACS Publications.

Table 3. Cu sulfides-based Z-schemes family heterojunctions for H_2 production (AQE: apparent quantum efficiency; SA: sacrificial agent; NA: not available).

Photocatalyst	Fabrication Methodology	Irradiation Source	H_2 Production Activity and AQE	Reference
$ZnO/ZnS/Cu_2S$	Sputtering–Sulfidation	Xe lamp (150 W, $\lambda \leq 400$ nm)	436 µmol g^{-1} h^{-1} AQE: 0.86% (420 nm) SA	[99]
$Cu_2S/ZnCdS$	Hydrothermal	5 W LED	5.9 mmol g^{-1} h^{-1} AQE: 2.13% (400 nm) SA	[100]
$Cu_2S/Zn_{0.67}C_{0.33}dS$	Hydrothermal	Xe lamp (300 W, $\lambda \geq 420$ nm)	15.3 mmol g^{-1} h^{-1} AQE: 18.15% (420 nm) SA	[101]
$CuS/Ag_2O/g\text{-}C_3N_4$	Hydrothermal–Precipitation	Solar simulator	1.8 mmol g^{-1} h^{-1} AQE: NA SA	[103]
CuS/CdS	Cation exchange	Xe lamp (300 W, $\lambda \geq 420$ nm)	13.4 mmol g^{-1} h^{-1} AQE: NA SA	[104]
$NiCo_2O_4/CuS$	Electrostatic self-assembly	Solar simulator	6.0 mmol g^{-1} h^{-1} AQE: NA SA	[105]
Cu_7S_4/MnS	Cation exchange	Xe lamp (300 W)	718 µmol g^{-1} h^{-1} AQE: 18.8% (420 nm) SA	[107]
Cu_7S_4/CdS	Cation exchange	Xe lamp (300 W, $\lambda \geq 420$ nm)	21.6 mmol g^{-1} h^{-1} AQE: 14.4% SA	[108]
$g\text{-}C_3N_4/CuInS_2$	Hydrothermal	Xe lamp (300 W, $\lambda \geq 420$ nm)	1.3 mmol g^{-1} h^{-1} AQE: 5.6% (400 nm) SA	[110]
$Au/CuInS_2/g\text{-}C_3N_4$	Impregnation/Photodeposition	Xe lamp (300 W)	10.7 mmol g^{-1} h^{-1} AQE: NA SA	[111]
$Pt\text{-}CuInS_2/CdS$	Impregnation	Xe lamp (300 W, $\lambda \geq 420$ nm)	20.5 µmol g^{-1} h^{-1} AQE: 0.3% (380 nm) SA	[112]
$Ti_3C_2/TiO_2/CuInS_2$	Hydrothermal	Xe lamp (300 W)	356.3 µmol g^{-1} h^{-1} AQE: 1.9% (350 nm) SA	[113]
$Cd_{0.5}Zn_{0.5}S/CuInS_2$	Solvothermal	Xe lamp (300 W, $\lambda \geq 420$ nm)	7.7 mmol g^{-1} h^{-1} AQE: 1.25% (420 nm) SA	[114]
$(CuGa)_{0.5}ZnS_2/RGO\text{-}(CoO_x/BiVO_4)$	Impregnation	Xe lamp (300 W, $\lambda \geq 420$ nm)	128 µmol g^{-1} h^{-1} AQE: 0.8% (440 nm) SA	[115]
$(CuGa)_{0.5}ZnS_2/(CoO_x/BiVO_4)$	Impregnation	Xe lamp (300 W, $\lambda \geq 420$ nm)	44.7 µmol g^{-1} h^{-1} AQE: NA SA	[116]

Table 3. *Cont.*

Photocatalyst	Fabrication Methodology	Irradiation Source	H$_2$ Production Activity and AQE	Reference
Cu$_2$NiSnS$_4$/TiO$_2$	Hydrothermal	Solar simulator	7.1 mmol g^{-1} h^{-1} AQE: NA SA	[117]
Cu$_2$ZnSnS$_4$/Cu$_2$O	Solvothermal	Xe lamp (300 W, $\lambda \geq 420$ nm)	897 µmol g^{-1} h^{-1} AQE: NA SA	[118]

3.3. Cu Phosphide-Based Z-Schemes (Family)

In the last five years, copper phosphide (Cu$_3$P) has attracted attention as a semi-conducting (p-type) and plasmonic material for its application in optical, electronic, and photocatalysis applications [119,120]. In this sense, Cu$_3$P is a p-type semiconductor material with a band gap of about 1.5 eV, indicating absorption in visible light [121]. Moreover, this semiconductor presents a suitable band alignment to perform the H$_2$ production from water splitting [119,121,122]. However, Cu$_3$P displays drawbacks for its application as a photocatalyst in overall water splitting reaction such as photocorrosion, rapid recombination of photo-induced e$^-$-h$^+$ pairs, and high oxidation potential. The fabrication of Z-Scheme heterojunctions represents a solution to solve these drawbacks [123,124]. A. Rauf et al. studied for the first time the pristine Cu$_3$P catalyst for solar watersplitting applications, indicating its potential. Moreover, they also observed that the construction by the ball milling method of a novel direct Z-scheme based on Cu$_3$P (Bi$_2$WO$_6$–Cu$_3$P) without a co-catalyst and mediator brings a higher photocatalytic activity in overall water splitting than the pure semiconductors (Bi$_2$WO$_6$ and Cu$_3$P). This work emphasizes the importance of materials design based on appropriate energy level positions to photocatalytically produce H$_2$ [125]. S. Hua et al. combined Cu$_3$P with the widely studied g-C$_3$N$_4$ nanosheets photocatalyst via chemical deposition and phosphorization, obtaining a novel Z-scheme based on the Cu$_3$P semiconductor (see Figure 5a). The reaction mechanism of the composite shows that Cu$_3$P enhances the charge separation process. Indeed, the authors revealed that the photogenerated e$^-$ in g-C$_3$N$_4$ recombine with the h$^+$ in Cu$_3$P, the photogenerated e$^-$ of Cu$_3$P will be left for H$_2$ production, improving the photocatalytic activity of the Z-scheme semiconductor (Figure 5a) [126]. Z. Yang et al. observed a boost in photocatalytic H$_2$ production using a 10 wt% Cu$_3$P/ZnIn$_2$S$_4$ Z-scheme synthesized by the facile solution-phase hybridization method as a photocatalyst, obtaining an apparent quantum yield of 22.3% at 420 nm (Figure 5b). The authors indicated that this fact might be related to the formation of Z-scheme with a built-in electric field within Cu$_3$P/ZnIn$_2$S$_4$ and Z-scheme charge carriers transfer pathway, which results in an efficient separation and migration of charge carriers. DFT-based DOS and PDOS are used to gain information about the electronic structure of the heterojunction. Charge-density profiles were used to indicate the charge transfer [127]. Q. Wang et al. demonstrated that a Z-scheme photocatalyst of Cu$_3$P with TiO$_2$ is feasible using a hydrothermal methodology. The authors show that the catalyst was active in visible light; see Figure 5c [128]. G. Ge et al. fabricated Cu$_3$P/Zn$_{0.5}$Cd$_{0.5}$S via an in situ phosphating method. The authors also observed that the Cu$_3$P/Zn$_{0.5}$Cd$_{0.5}$S Z-scheme heterojunction increased the H$_2$ production, which is 3.1 folds higher than Zn$_{0.5}$Cd$_{0.5}$S due to a strong contact between Cu$_3$P and Zn$_{0.5}$Cd$_{0.5}$S introduced by in situ phosphidation method [129].

Another alternative to ensure the efficient transmission of photogenerated carriers and further optimize the structure of the Z-scheme family systems is the design of dual-Z-scheme systems. [130]. In this sense, K. Wang et al. designed for the first time a metal-organic frameworks (MOF)-derived dual-S-scheme based on Cu$_3$P by simple hydrothermal and phosphating methods (Figure 5d). The authors indicated that the optimized CoP/Cu$_3$P/Ni$_2$P (CCNP) photocatalyst had a photocatalytic hydrogen evolution activity of 786.58 µmol g^{-1} h^{-1}, which is roughly 2.64 and 3.33 times higher than that of CoP (CP)

and CoP/Ni$_2$P (CNP), respectively. This work opens the door for the use of dual S-schemes based on the Cu$_3$P photocatalyst in H$_2$ production [131] (Table 4).
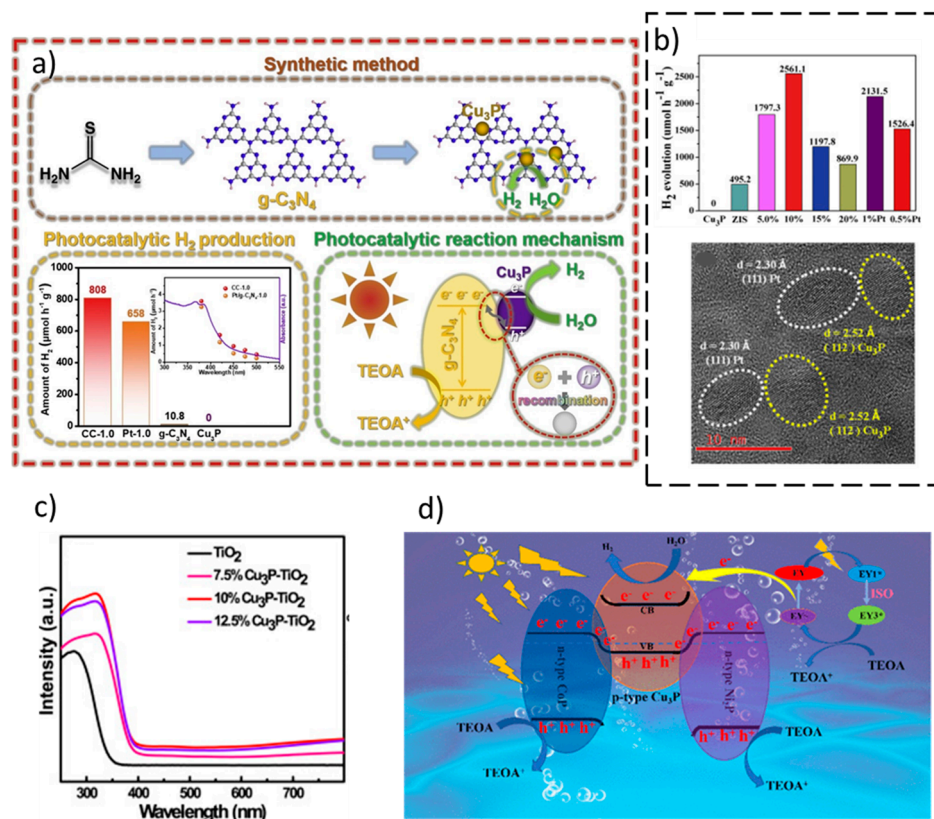
Figure 5. (**a**) Synthetic method, photocatalytic H$_2$ production, and photocatalytic reaction mechanism of the Cu$_3$P/g-C$_3$N$_4$ heterojunction synthesized by phosphorization. Reproduced from [126]. Copyright 2019, Elsevier. (**b**) Photocatalytic production of Cu$_3$P/ZnIn$_2$S$_4$ photocatalyst and TEM images of the composite showing the intimate contact between the semiconductors. Reproduced from [127]. Copyright 2020, Elsevier. (**c**) UV-visible spectra of Cu$_3$P/TiO$_2$ active photocatalysts. Reproduced from [128]. Copyright 2022, Elsevier. (**d**) Photocatalytic reaction mechanism of CoP/Cu$_3$P/Ni$_2$P dual S-scheme. Reproduced from [131]. Copyright 2022, ACS Publications.

3.4. Other Cu-Based Z-Schemes (Family)

Along with the most common Cu-based compounds described up to now, different materials have been used to construct Z-schemes family heterojunctions, i.e., CuI, Cu-based metal-organic frameworks (MOFs), and multimetallic compounds. In this section, we will briefly describe some of them and their properties. Their photocatalytic performances are resumed in Table 5.

CuI has been drawing attention for its high hole mobility and applicability in optoelectronic applications, but it has a wide band gap (3.1 eV) [132], different from all the compounds that we are observing in this review. This band gap makes mandatory the use of narrow band gap semiconductors if it is intended to use this compound in visible light-mediated processes. Up to now, this interesting material has been used in combination with graphdiyne (GDY) to decrease its recombination rate and simplify the synthetic approach to obtain GDY. It was possible to obtain different S-schemes in combination with several semiconductors, i.e., Co$_9$S$_8$ (see Figure 6a) [133], CdS [134], MIL-53 [135], NiTiO$_3$ [136], Co$_3$(PO$_4$)$_2$ [137], CoFe layered hydroxide (LDH) [138], NiV LDH [139], and MoO$_2$ [140] active in H$_2$ production.

Table 4. Cu phosphide-based Z-schemes family heterojunctions for H_2 production (AQE: apparent quantum efficiency; SA: sacrificial agent; NA: not available).

Photocatalyst	Fabrication Methodology	Irradiation Source	H_2 Production Activity (μmol g^{-1} h^{-1}) and AQE	Reference
Bi$_2$WO6-Cu3P	Mechanical ball milling	Xe lamp (AM 1.5G)	40.6 AQE: NA SA	[125]
Cu$_3$P/g-C$_3$N$_4$	Phosphorization	Xe lamp (300 W, $\lambda \geq$ 420 nm)	808 AQE: NA SA	[126]
Cu$_3$P/ZnIn$_2$S$_4$	Solution-phase hybridization method	Xe lamp (300 W, $\lambda \geq$ 420 nm)	2561.1 AQE: NA AQE: 22.3% (420 nm) SA	[127]
Cu$_3$P/TiO2	Hydrothermal method	Xe lamp (300 W, $\lambda \geq$ 420 nm)	607.5 AQE: NA SA	[128]
Cu$_3$P/Zn0.5Cd0.5S	In situ phosphidation method	Xe lamp (300 W, $\lambda \geq$ 420 nm)	2700 AQE: NA SA	[129]
CoP/Cu3P/Ni2P	Hydrothermal and phosphating	5 W LED white light ($\lambda \geq$ 420 nm)	786.58 AQE: 3.69% (420 nm) SA	[131]

MOFs are not semiconductors, but their structural tunability makes them interesting for the efficient use of solar light in several photocatalytic applications [141]. Cu-based MOFs have been used in S-schemes to improve the active sites of different semiconductors. Cao et al. used Cu-MOFs to construct an active heterojunction with Mn$_{0.05}$Cd$_{0.95}$S by improving the surface chemistry of the materials and its optical properties, as shown in Figure 6b [142]. Similarly, a Cu-MOF was used to enhance the photocatalytic activity of CdS, improving not only the surface area but also the charge carriers' separation [143].

Finally, the synergistic effect of the use of Cu in the presence of other metals has been exploited not only in oxides and sulfides but also in mixed-transition metal oxysulfides. Sun et al. used La$_5$Ti$_2$Cu$_{0.9}$Ag$_{0.1}$S$_5$O$_7$ to improve the photocatalytic activity of BiVO$_4$ in a Z-scheme for the overall water splitting and decrease the undesired redox reactions common in oxysulfides [144].
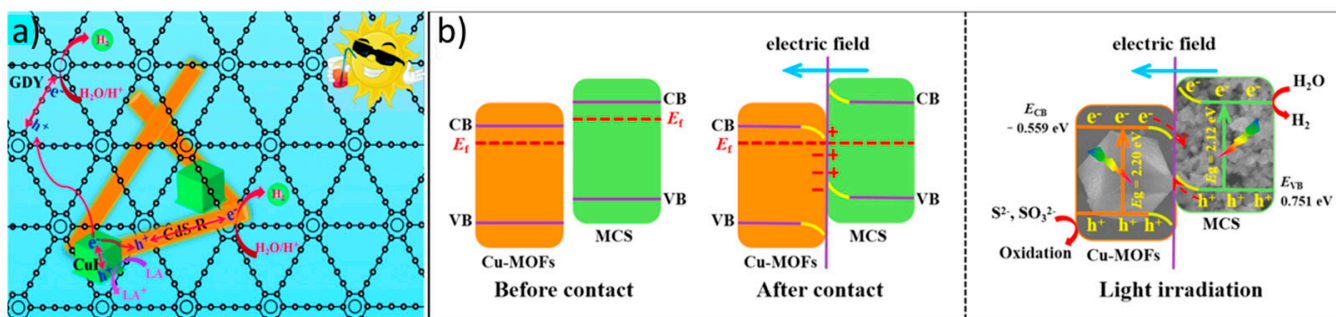
Figure 6. (**a**) Photocatalytic H_2 generation mechanism of the hybrid catalyst GDY/CuI/CdS- R. Reproduced from [144]. Copyright 2022, RSC Publications (**b**) Photocatalytic mechanism of the Cu-MOFs/Mn$_{0.05}$Cd$_{0.95}$S. Reproduced from [142]. Copyright 2021, Elsevier.

Table 5. Other Cu-based Z-schemes family heterojunctions for H_2 production (AQE: apparent quantum efficiency; SA: sacrificial agent; NA: not available).

Photocatalyst	Fabrication Methodology	Irradiation Source	H_2 Production Activity and AQE	Reference
Co_9S_8/GDY/CuI	Hydrothermal	5 W LED	1.4 mmol g^{-1} h^{-1} AQE: NA SA	[133]
CuI/GDY/CdS-R	Hydrothermal	5 W LED	16.2 mmol g^{-1} h^{-1} AQE: 6.11% (450 nm) SA	[134]
GDY/CuI/MIL-53	Ultrasonication	5 W LED	596.8 µmol g^{-1} h^{-1} AQE: NA SA	[135]
GDY/CuI/NiTiO$_3$	Impregnation	5 W LED	509.03 µmol g^{-1} h^{-1} AQE: NA SA	[136]
$Co_3(PO_4)_2$/CuI/GDY	Hot solvent	5 W LED	319.4 µmol g^{-1} h^{-1} AQE: NA SA	[137]
CoFe LDH/CuI/GDY	Solvothermal	5 W LED	1.2 mmol g^{-1} h^{-1} AQE: NA SA	[138]
GDY/CuI/NiV LDH	Hot solvent	5 W LED	2.9 mmol g^{-1} h^{-1} AQE: 0.15% (420 nm) SA	[139]
GDY/CuI/MoO$_2$	Hot solvent	5 W LED	820 µmol g^{-1} h^{-1} AQE: 4.2% (520 nm) SA	[140]
Cu-MOF/$Mn_{0.05}Cd_{0.95}S$	Hydrothermal	5 W LED	13.7 mmol g^{-1} h^{-1} AQE: 1.83% (450 nm) SA	[142]
Cu-MOF/CdS	Impregnation	5 W LED	4 mmol g^{-1} h^{-1} AQE: NA SA	[143]
$La_5Ti_2Cu_{0.9}Ag_{0.1}S_5O_7$/BiVO$_4$	Particle transfer	Xe lamp (300 W, $\lambda \geq 420$ nm)	2.75 µmol cm^{-2} h^{-1} AQE: 4.9% (420 nm) SA	[144]

4. Conclusions and Outlooks

In conclusion, Cu-based Z-schemes family photocatalysts are an innovative technology to boost the H_2 production activity and to overcome the main drawbacks of the single photocatalysts, i.e., high e^--h^+ recombination rate, photocorrosion, and inadequate redox potentials. Moreover, the use of a transition metal such as Cu favors the possibility of their future commercial application due to the low cost and the photocatalytic activity properties of Cu. In this review, a comprehensive overview of the recent research on Cu-based Z-schemes family photocatalysts for their use in solar photocatalytic H_2 production is described. The scientific community has developed several synthetic methodologies and combinations with different semiconductors to boost the catalytic properties of the synthesized materials. In this sense, researchers combined different compounds of Cu (copper oxide, copper sulfide, etc.) with widely studied semiconductors (TiO_2, g-C_3N_4, MOFs, etc.), and the results described in this review show that the Z-schemes obtained present higher activity than the pristine Cu-based semiconductors. This fact indicates the important role

of this system in removing the photocorrosion and improving the charge transfer of the Cu-based semiconductors for their future application in the industry. However, nowadays, the photocatalytic efficiencies are still low, and many catalytic mechanisms remain unclear, being the main drawbacks for their commercialization. With this in mind, the challenges for new researchers in the application of Cu-based Z-schemes family photocatalysts might be in the synthetic methodology, focusing on the interaction between the Cu-based semiconductor and the other semiconductor in the heterojunction. The use of ab initio calculations is not only to describe but also to yield conclusions; neither is it justified to use a partial study to support claims. There is an important need for a thorough study of systems to gain deep insights into the systems studied experimentally. As mentioned in this review, the intimate contact between both components is one of the keys to improving the photocatalytic activity of the heterostructures and obtaining Z-schemes systems. Additionally, the monitoring of the reaction has a central role, but it is sometimes complex due to the formation of by-products or photocorrosion of the catalyst. Hence, it is also necessary to perform in-depth studies of the catalytic reactions' mechanisms and, to do so, in all the stages of these catalytic processes (adsorption, reaction, and desorption). To this end, ab initio calculations can help in giving directions for the determination of the atomic reactivity of catalysts. This opens the doors to developing novel Cu-based Z-scheme photocatalysts, characterization techniques, and studies of new mechanisms to obtain catalysts capable of being soon used in practical applications using solar light. Another drawback that should be addressed by the scientific community to the commercialization of this technology is the design and the manufacture of stable photocatalysts under reaction conditions since most of the works reported do not study in deep the stability of the catalyst used.

References

1. Panwar, N.L.; Kaushik, S.C.; Kothari, S. Role of Renewable Energy Sources in Environmental Protection: A Review. *Renew. Sustain. Energy Rev.* **2011**, *15*, 1513–1524. [CrossRef]
2. Ahmad, T.; Zhang, D. A Critical Review of Comparative Global Historical Energy Consumption and Future Demand: The Story Told so Far. *Energy Rep.* **2020**, *6*, 1973–1991. [CrossRef]
3. Chen, C.; Pinar, M.; Stengos, T. Renewable Energy Consumption and Economic Growth Nexus: Evidence from a Threshold Model. *Energy Policy* **2020**, *139*, 111295. [CrossRef]
4. Jain, I.P. Hydrogen the Fuel for 21st Century. *Int. J. Hydrogen Energy* **2009**, *34*, 7368–7378. [CrossRef]
5. Abdin, Z.; Zafaranloo, A.; Rafiee, A.; Mérida, W.; Lipiński, W.; Khalilpour, K.R. Hydrogen as an Energy Vector. *Renew. Sustain. Energy Rev.* **2020**, *120*, 109620. [CrossRef]
6. Lubitz, W.; Tumas, W. Hydrogen: An Overview. *Chem. Rev.* **2007**, *107*, 3900–3903. [CrossRef]
7. Osman, A.I.; Mehta, N.; Elgarahy, A.M.; Hefny, M.; Al-Hinai, A.; Al-Muhtaseb, A.H.; Rooney, D.W. *Hydrogen Production, Storage, Utilisation and Environmental Impacts: A Review*; Springer International Publishing: Midtown Manhattan, NY, USA, 2022; Volume 20, ISBN 0123456789.
8. Sazali, N. Emerging Technologies by Hydrogen: A Review. *Int. J. Hydrogen Energy* **2020**, *45*, 18753–18771. [CrossRef]
9. Jafari, T.; Moharreri, E.; Amin, A.S.; Miao, R.; Song, W.; Suib, S.L. Photocatalytic Water Splitting—The Untamed Dream: A Review of Recent Advances. *Molecules* **2016**, *21*, 900. [CrossRef]

10. Fajrina, N.; Tahir, M. A Critical Review in Strategies to Improve Photocatalytic Water Splitting towards Hydrogen Production. *Int. J. Hydrogen Energy* **2019**, *44*, 540–577. [CrossRef]

11. Li, R.; Li, C. Chapter One—Photocatalytic Water Splitting on Semiconductor-Based Photocatalysts. In *Advances in Catalysis*; Academic Press: Cambridge, MA, USA, 2017; Volume 60, pp. 1–57.

12. Kudo, A.; Miseki, Y. Heterogeneous photocatalyst materials for water splitting. *Chem. Soc. Rev.* **2009**, *38*, 253–278. [CrossRef]

13. Maeda, K. Photocatalytic Water Splitting Using Semiconductor Particles: History and Recent Developments. *J. Photochem. Photobiol. C Photochem. Rev.* **2011**, *12*, 237–268. [CrossRef]

14. Schneider, J.; Matsuoka, M.; Takeuchi, M.; Zhang, J.; Horiuchi, Y.; Anpo, M.; Bahnemann, D.W. Understanding TiO_2 Photocatalysis Mechanisms and Materials. *Chem. Rev.* **2014**, *114*, 9919–9986. [CrossRef] [PubMed]

15. Wang, Q.; Domen, K. Particulate Photocatalysts for Light-Driven Water Splitting: Mechanisms, Challenges, and Design Strategies. *Chem. Rev.* **2020**, *120*, 919–985. [CrossRef] [PubMed]

16. Fujishima, A.; Honda, K. Electrochemical Photolysis of Water at a Semiconductor Electrode. *Nature* **1972**, *238*, 37–38. [CrossRef] [PubMed]

17. Dong, H.; Zeng, G.; Tang, L.; Fan, C.; Zhang, C.; He, X.; He, Y. An Overview on Limitations of TiO_2-Based Particles for Photocatalytic Degradation of Organic Pollutants and the Corresponding Countermeasures. *Water Res.* **2015**, *79*, 128–146. [CrossRef]

18. Peiris, S.; de Silva, H.B.; Ranasinghe, K.N.; Bandara, S.V.; Perera, I.R. Recent Development and Future Prospects of TiO_2 Photocatalysis. *J. Chin. Chem. Soc.* **2021**, *68*, 738–769. [CrossRef]

19. Zhang, H.; Liu, J.; Xu, T.; Ji, W.; Zong, X. Recent Advances on Small Band Gap Semiconductor Materials ($\leq$2.1 EV) for Solar Water Splitting. *Catalysts* **2023**, *13*, 728. [CrossRef]

20. Sumesh, C.K.; Peter, S.C. Two-Dimensional Semiconductor Transition Metal Based Chalcogenide Based Heterostructures for Water Splitting Applications. *Dalt. Trans.* **2019**, *48*, 12772–12802. [CrossRef]

21. Mikaeili, F.; Gilmore, T.; Gouma, P.I. Photochemical Water Splitting via Transition Metal Oxides. *Catalysts* **2022**, *12*, 1303. [CrossRef]

22. Zindrou, A.; Belles, L.; Deligiannakis, Y. Cu-Based Materials as Photocatalysts for Solar Light Artificial Photosynthesis: Aspects of Engineering Performance, Stability, Selectivity. *Solar* **2023**, *3*, 87–112. [CrossRef]

23. Xie, H.; Wang, J.; Ithisuphalap, K.; Wu, G.; Li, Q. Recent Advances in Cu-Based Nanocomposite Photocatalysts for CO_2 Conversion to Solar Fuels. *J. Energy Chem.* **2017**, *26*, 1039–1049. [CrossRef]

24. Gawande, M.B.; Goswami, A.; Felpin, F.X.; Asefa, T.; Huang, X.; Silva, R.; Zou, X.; Zboril, R.; Varma, R.S. Cu and Cu-Based Nanoparticles: Synthesis and Applications in Catalysis. *Chem. Rev.* **2016**, *116*, 3722–3811. [CrossRef] [PubMed]

25. Kumar, M.; Meena, B.; Subramanyam, P.; Suryakala, D.; Subrahmanyam, C. Emerging Copper-Based Semiconducting Materials for Photocathodic Applications in Solar Driven Water Splitting. *Catalysts* **2022**, *12*, 1198. [CrossRef]

26. Amorós-Pérez, A.; Cano-Casanova, L.; Castillo-Deltell, A.; Lillo-Ródenas, M.Á.; Román-Martínez, M.d.C. TiO2 Modification with Transition Metallic Species (Cr, Co, Ni, and Cu) for Photocatalytic Abatement of Acetic Acid in Liquid Phase and Propene in Gas Phase. *Materials* **2019**, *12*, 40. [CrossRef]

27. Fernández-Catalá, J.; Navlani-García, M.; Verma, P.; Berenguer-Murcia, Á.; Mori, K.; Kuwahara, Y.; Yamashita, H.; Cazorla-Amorós, D. Photocatalytically-driven H_2 production over Cu/TiO_2 catalysts decorated with multi-walled carbon nanotubes. *Catal. Today* **2021**, *364*, 182–189. [CrossRef]

28. Cao, Q.; Che, R.; Chen, N. Scalable synthesis of Cu_2S double-superlattice nanoparticle systems with enhanced UV/visible-light-driven photocatalytic activity. *Appl. Catal. B.* **2015**, *162*, 187–195. [CrossRef]

29. Luo, J.; Dai, Z.; Feng, M.; Gu, M.; Xie, Y. Graphitic carbon nitride/ferroferric oxide/reduced graphene oxide nanocomposite as highly active visible light photocatalyst. *Nano Res.* **2023**, *16*, 371–376. [CrossRef]

30. Janczarek, M.; Kowalska, E. On the Origin of Enhanced Photocatalytic Activity of Copper-Modified Titania in the Oxidative Reaction Systems. *Catalysts* **2017**, *7*, 318. [CrossRef]

31. Chen, P.; Zhang, P.; Cui, Y.; Fu, X.; Wang, Y. Recent Progress in Copper-Based Inorganic Nanostructure Photocatalysts: Properties, Synthesis and Photocatalysis Applications. *Mater. Today Sustain.* **2023**, *21*, 100276. [CrossRef]

32. Wang, W.; Wang, L.; Su, W.; Xing, Y. Photocatalytic CO_2 reduction over Copper-Based Materials: A Review. *J. CO2 Util.* **2022**, *61*, 102056. [CrossRef]

33. Aguirre, M.E.; Zhou, R.; Eugene, A.J.; Guzman, M.I.; Grela, M.A. Cu_2O/TiO_2 Heterostructures for CO_2 Reduction through a Direct Z-Scheme: Protecting Cu_2O from Photocorrosion. *Appl. Catal. B Environ.* **2017**, *217*, 485–493. [CrossRef]

34. Toe, C.Y.; Scott, J.; Amal, R.; Ng, Y.H. Recent Advances in Suppressing the Photocorrosion of Cuprous Oxide for Photocatalytic and Photoelectrochemical Energy Conversion. *J. Photochem. Photobiol. C Photochem. Rev.* **2019**, *40*, 191–211. [CrossRef]

35. Zhang, W.; Chen, X.; Zhao, X.; Yin, M.; Feng, L.; Wang, H. Simultaneous Nitrogen Doping and Cu_2O Oxidization by One-Step Plasma Treatment toward Nitrogen-Doped Cu_2O@CuO Heterostructure: An Efficient Photocatalyst for H_2O_2 Evolution under Visible Light. *Appl. Surf. Sci.* **2020**, *527*, 146908. [CrossRef]

36. Lai, T.H.; Tsao, C.W.; Fang, M.J.; Wu, J.Y.; Chang, Y.P.; Chiu, Y.H.; Hsieh, P.Y.; Kuo, M.Y.; Chang, K.D.; Hsu, Y.J. Au@Cu_2O Core-Shell and Au@Cu_2Se Yolk-Shell Nanocrystals as Promising Photocatalysts in Photoelectrochemical Water Splitting and Photocatalytic Hydrogen Production. *ACS Appl. Mater. Interfaces* **2022**, *14*, 40771–40783. [CrossRef] [PubMed]

37. Alizadeh, M.; Tong, G.B.; Qadir, K.W.; Mehmood, M.S.; Rasuli, R. Cu$_2$O/InGaN Heterojunction Thin Films with Enhanced Photoelectrochemical Activity for Solar Water Splitting. *Renew. Energy* **2020**, *156*, 602–609. [CrossRef]

38. Xi, Z.; Li, C.; Zhang, L.; Xing, M.; Zhang, J. Synergistic Effect of Cu$_2$O/TiO$_2$ Heterostructure Nanoparticle and Its High H$_2$ Evolution Activity. *Int. J. Hydrogen Energy* **2014**, *39*, 6345–6353. [CrossRef]

39. Tian, L.; Guan, X.; Zong, S.; Dai, A.; Qu, J. Cocatalysts for Photocatalytic Overall Water Splitting: A Mini Review. *Catalysts* **2023**, *13*, 355. [CrossRef]

40. Maeda, K.; Teramura, K.; Lu, D.; Saito, N.; Inoue, Y.; Domen, K. Noble Metal/Cr$_2$O$_3$ Core/Shell Nanoparticles as a Cocatalyst for Photocatalytic Overall Water Splitting. *Angew. Chem. Int. Ed.* **2006**, *45*, 7806–7809. [CrossRef]

41. Wang, Y.; Suzuki, H.; Xie, J.; Tomita, O.; Martin, D.J.; Higashi, M.; Kong, D.; Abe, R.; Tang, J. Mimicking Natural Photosynthesis: Solar to Renewable H$_2$ Fuel Synthesis by Z-Scheme Water Splitting Systems. *Chem. Rev.* **2018**, *118*, 5201–5241. [CrossRef]

42. Dogutan, D.K.; Nocera, D.G. Artificial Photosynthesis at Efficiencies Greatly Exceeding That of Natural Photosynthesis. *Acc. Chem. Res.* **2019**, *52*, 3143–3148. [CrossRef]

43. Xu, Q.; Zhang, L.; Yu, J.; Wageh, S.; Al-Ghamdi, A.A.; Jaroniec, M. Direct Z-Scheme Photocatalysts: Principles, Synthesis, and Applications. *Mater. Today* **2018**, *21*, 1042–1063. [CrossRef]

44. Xu, Q.; Zhang, L.; Cheng, B.; Fan, J.; Yu, J. S-Scheme Heterojunction Photocatalyst. *Chem* **2020**, *6*, 1543–1559. [CrossRef]

45. Abdul Nasir, J.; Munir, A.; Ahmad, N.; Haq, T.; Khan, Z.; Rehman, Z. Photocatalytic Z-Scheme Overall Water Splitting: Recent Advances in Theory and Experiments. *Adv. Mater.* **2021**, *33*, 1–41. [CrossRef]

46. Fernández-Catalá, J.; Greco, R.; Navlani-García, M.; Cao, W.; Berenguer-Murcia, Á.; Cazorla-Amorós, D. g-C$_3$N$_4$-Based Direct Z-Scheme Photocatalysts for Environmental Applications. *Catalysts* **2022**, *12*, 1137. [CrossRef]

47. Huang, D.; Chen, S.; Zeng, G.; Gong, X.; Zhou, C.; Cheng, M.; Xue, W.; Yan, X.; Li, J. Artificial Z-Scheme Photocatalytic System: What Have Been Done and Where to Go? *Coord. Chem. Rev.* **2019**, *385*, 44–80. [CrossRef]

48. Kumar, R.; Sudhaik, A.; Khan, A.A.P.; Raizada, P.; Asiri, A.M.; Mohapatra, S.; Thakur, S.; Thakur, V.K.; Singh, P. Current Status on Designing of Dual Z-Scheme Photocatalysts for Energy and Environmental Applications. *J. Ind. Eng. Chem.* **2022**, *106*, 340–355. [CrossRef]

49. Jing, D.; Guo, L.; Zhao, L.; Zhang, X.; Liu, H.; Li, M.; Shen, S.; Liu, G.; Hu, X.; Zhang, X.; et al. Efficient Solar Hydrogen Production by Photocatalytic Water Splitting: From Fundamental Study to Pilot Demonstration. *Int. J. Hydrogen Energy* **2010**, *35*, 7087–7097. [CrossRef]

50. Nishiyama, H.; Yamada, T.; Nakabayashi, M.; Maehara, Y.; Yamaguchi, M.; Kuromiya, Y.; Nagatsuma, Y.; Tokudome, H.; Akiyiyama, S.; Watanabe, T.; et al. Photocatalytic Solar Hydrogen Production from Water on a 100-m^2 Scale. *Nature* **2021**, *598*, 304–307. [CrossRef]

51. Marschall, R. Semiconductor Composites: Strategies for Enhancing Charge Carrier Separation to Improve Photocatalytic Activity. *Adv. Funct. Mater.* **2014**, *24*, 2421–2440. [CrossRef]

52. Saravanan, A.; Kumar, P.S.; Vo, D.V.N.; Yaashikaa, P.R.; Karishma, S.; Jeevanantham, S.; Gayathri, B.; Bharathi, V.D. Photocatalysis for Removal of Environmental Pollutants and Fuel Production: A Review. *Environ. Chem. Lett.* **2021**, *19*, 441–463. [CrossRef]

53. Zhang, W.; Mohamed, A.R.; Ong, W.J. Z-Scheme Photocatalytic Systems for Carbon Dioxide Reduction: Where Are We Now? *Angew. Chem. Int. Ed.* **2020**, *59*, 22894–22915. [CrossRef]

54. Zhao, Y.; Linghu, X.; Shu, Y.; Zhang, J.; Chen, Z.; Wu, Y.; Shan, D.; Wang, B. Classification and Catalytic Mechanisms of Heterojunction Photocatalysts and the Application of Titanium Dioxide (TiO$_2$)-Based Heterojunctions in Environmental Remediation. *J. Environ. Chem. Eng.* **2022**, *10*, 108077. [CrossRef]

55. Muscetta, M.; Andreozzi, R.; Clarizia, L.; Di Somma, I.; Marotta, R. Hydrogen Production through Photoreforming Processes over Cu$_2$O/TiO$_2$ Composite Materials: A Mini-Review. *Int. J. Hydrogen Energy* **2020**, *45*, 28531–28552. [CrossRef]

56. Liao, G.; Li, C.; Liu, S.Y.; Fang, B.; Yang, H. Z-Scheme Systems: From Fundamental Principles to Characterization, Synthesis, and Photocatalytic Fuel-Conversion Applications. *Phys. Rep.* **2022**, *983*, 1–41. [CrossRef]

57. Christoforidis, K.C.; Fornasiero, P. Photocatalysis for Hydrogen Production and CO$_2$ Reduction: The Case of Copper-Catalysts. *ChemCatChem* **2019**, *11*, 368–382. [CrossRef]

58. Wang, L.; Bie, C.; Yu, J. Challenges of Z-scheme photocatalytic mechanisms. *Trends Chem.* **2022**, *4*, 973–983. [CrossRef]

59. Bard, A.J. Photoelectrochemistry and Heterogeneous Photo-Catalysis at Semiconductors. *J. Photochem.* **1979**, *10*, 59–75. [CrossRef]

60. Jourshabani, M.; Lee, B.K.; Shariatinia, Z. From Traditional Strategies to Z-Scheme Configuration in Graphitic Carbon Nitride Photocatalysts: Recent Progress and Future Challenges. *Appl. Catal. B Environ.* **2020**, *276*, 119157. [CrossRef]

61. Tada, H.; Mitsui, T.; Kiyonaga, T.; Akita, T.; Tanaka, K. All-Solid-State Z-Scheme in CdS-Au-TiO$_2$ Three-Component Nanojunction System. *Nat. Mater.* **2006**, *5*, 782–786. [CrossRef] [PubMed]

62. Zhou, P.; Yu, J.; Jaroniec, M. All-Solid-State Z-Scheme Photocatalytic Systems. *Adv. Mater.* **2014**, *26*, 4920–4935. [CrossRef] [PubMed]

63. Yuan, Y.; Guo, R.T.; Hong, L.F.; Ji, X.Y.; Lin, Z.D.; Li, Z.S.; Pan, W.G. A Review of Metal Oxide-Based Z-Scheme Heterojunction Photocatalysts: Actualities and Developments. *Mater. Today Energy* **2021**, *21*, 100829. [CrossRef]

64. Yu, J.; Wang, S.; Low, J.; Xiao, W. Enhanced Photocatalytic Performance of Direct Z-Scheme g-C$_3$N$_4$-TiO$_2$ Photocatalysts for the Decomposition of Formaldehyde in Air. *Phys. Chem. Chem. Phys.* **2013**, *15*, 16883–16890. [CrossRef] [PubMed]

65. Kumar, A.; Khosla, A.; Kumar Sharma, S.; Dhiman, P.; Sharma, G.; Gnanasekaran, L.; Naushad, M.; Stadler, F.J. A Review on S-Scheme and Dual S-Scheme Heterojunctions for Photocatalytic Hydrogen Evolution, Water Detoxification and CO_2 Reduction. *Fuel* **2023**, *333*, 126267. [CrossRef]

66. Bao, Y.; Song, S.; Yao, G.; Jiang, S. S-Scheme Photocatalytic Systems. *Sol. RRL* **2021**, *5*, 2100118. [CrossRef]

67. Mohammed, A.M.; Mohtar, S.S.; Aziz, F.; Mhamad, S.A.; Aziz, M. Review of Various Strategies to Boost the Photocatalytic Activity of the Cuprous Oxide-Based Photocatalyst. *J. Environ. Chem. Eng.* **2021**, *9*, 105138. [CrossRef]

68. Hernández-Alonso, M.D.; Fresno, F.; Suárez, S.; Coronado, J.M. Development of Alternative Photocatalysts to TiO_2: Challenges and Opportunities. *Energy Environ. Sci.* **2009**, *2*, 1231–1257. [CrossRef]

69. Wei, T.; Zhu, Y.N.; An, X.; Liu, L.M.; Cao, X.; Liu, H.; Qu, J. Defect Modulation of Z-Scheme TiO_2/Cu_2O Photocatalysts for Durable Water Splitting. *ACS Catal.* **2019**, *9*, 8346–8354. [CrossRef]

70. Lv, S.; Wang, Y.; Zhou, Y.; Liu, Q.; Song, C.; Wang, D. Oxygen Vacancy Stimulated Direct Z-Scheme of Mesoporous Cu_2O/TiO_2 for Enhanced Photocatalytic Hydrogen Production from Water and Seawater. *J. Alloys Compd.* **2021**, *868*, 159144. [CrossRef]

71. Fu, J.; Cao, S.; Yu, J. Dual Z-Scheme Charge Transfer in TiO_2–Ag–Cu_2O Composite for Enhanced Photocatalytic Hydrogen Generation. *J. Mater.* **2015**, *1*, 124–133. [CrossRef]

72. Zhu, H.; Zhen, C.; Chen, X.; Feng, S.; Li, B.; Du, Y.; Liu, G.; Cheng, H.M. Patterning Alternate TiO_2 and Cu_2O Strips on a Conductive Substrate as Film Photocatalyst for Z-Scheme Photocatalytic Water Splitting. *Sci. Bull.* **2022**, *67*, 2420–2427. [CrossRef]

73. Ong, C.B.; Ng, L.Y.; Mohammad, A.W. A Review of ZnO Nanoparticles as Solar Photocatalysts: Synthesis, Mechanisms and Applications. *Renew. Sustain. Energy Rev.* **2018**, *81*, 536–551. [CrossRef]

74. Park, B.H.; Park, H.; Kim, T.; Yoon, S.J.; Kim, Y.; Son, N.; Kang, M. S-Scheme Assisted Cu_2O/ZnO Flower-Shaped Heterojunction Catalyst for Breakthrough Hydrogen Evolution by Water Splitting. *Int. J. Hydrogen Energy* **2021**, *46*, 38319–38335. [CrossRef]

75. Yoo, H.; Kahng, S.; Hyeun Kim, J. Z-Scheme Assisted ZnO/Cu_2O-CuO Photocatalysts to Increase Photoactive Electrons in Hydrogen Evolution by Water Splitting. *Sol. Energy Mater. Sol. Cells* **2020**, *204*, 110211. [CrossRef]

76. Xu, B.; Wang, B.; Zhang, H.; Yang, P. Z-Scheme Cu_2O Nanoparticle/Graphite Carbon Nitride Nanosheet Heterojunctions for Photocatalytic Hydrogen Evolution. *ACS Appl. Nano Mater.* **2022**, *5*, 8475–8483. [CrossRef]

77. Dai, B.; Li, Y.; Xu, J.; Sun, C.; Li, S.; Zhao, W. Photocatalytic Oxidation of Tetracycline, Reduction of Hexavalent Chromium and Hydrogen Evolution by Cu_2O/g-C_3N_4 S-Scheme Photocatalyst: Performance and Mechanism Insight. *Appl. Surf. Sci.* **2022**, *592*, 153309. [CrossRef]

78. Mahzoon, S.; Haghighi, M.; Nowee, M.; Zeinalzdeh, H. Sonoprecipitation Design of Novel Efficient All-Solid Z-Scheme $Cu(OH)_2/Cu_2O/C_3N_4$ Nanophotocatalyst Applied in Water Splitting for H_2 Production: Synergetic Effect of Cu-Based Cocatalyst $(Cu(OH)_2)$ and Electron Mediator (Cu). *Sol. Energy Mater. Sol. Cells* **2021**, *219*, 110772. [CrossRef]

79. Gu, Y.; Bao, A.; Zhang, X.; Yan, J.; Du, Q.; Zhang, M.; Qi, X. Facile Fabrication of Sulfur-Doped Cu_2O and g-C_3N_4 with Z-Scheme Structure for Enhanced Photocatalytic Water Splitting Performance. *Mater. Chem. Phys.* **2021**, *266*, 124542. [CrossRef]

80. Mu, F.; Miao, X.; Cao, J.; Zhao, W.; Yang, G.; Zeng, H.; Li, S.; Sun, C. Integration of Plasmonic Effect and S-Scheme Heterojunction into Gold Decorated Carbon Nitride/Cuprous Oxide Catalyst for Photocatalysis. *J. Clean. Prod.* **2022**, *360*, 131948. [CrossRef]

81. Shen, H.; Liu, G.; Yan, X.; Jiang, J.; Hong, Y.; Yan, M.; Mao, B.; Li, D.; Fan, W.; Shi, W. All-Solid-State Z-Scheme System of RGO-Cu_2O/Fe_2O_3 for Simultaneous Hydrogen Production and Tetracycline Degradation. *Mater. Today Energy* **2017**, *5*, 312–319. [CrossRef]

82. Shen, H.; Liu, G.; Zhao, Y.; Li, D.; Jiang, J.; Ding, J.; Mao, B.; Shen, H.; Kim, K.S.; Shi, W. Artificial All-Solid-State System by RGO Bridged Cu_2O and Bi_2WO_6 for Z-Scheme H_2 Production and Tetracycline Degradation. *Fuel* **2020**, *259*, 116311. [CrossRef]

83. Mohammed Ali, M.J.; Radhy, M.M.; Mashkoor, S.J.; Ali, E.M. Synthesis and Characterization of Copper Oxide Nanoparticles and Their Application for Solar Cell. *Mater. Today Proc.* **2022**, *60*, 917–921. [CrossRef]

84. Li, B.; Wang, Y.; Zeng, Y.; Wang, R. Synthesis of CuO Micro-Sphere Combined with g-C_3N_4 Using Cu_2O as Precursor for Enhanced Photocatalytic Hydrogen Evolution. *Mater. Lett.* **2016**, *178*, 308–311. [CrossRef]

85. Chu, S.; Hu, Y.; Zhang, J.; Cui, Z.; Shi, J.; Wang, Y.; Zou, Z. Constructing Direct Z-Scheme CuO/PI Heterojunction for Photocatalytic Hydrogen Evolution from Water under Solar Driven. *Int. J. Hydrogen Energy* **2021**, *46*, 9064–9076. [CrossRef]

86. Dai, L.; Sun, F.; Fu, P.; Li, H. Enhanced Photocatalytic Hydrogen Evolution and Ammonia Sensitivity of Double-Heterojunction g-$C3N_4/TiO_2$/CuO. *RSC Adv.* **2022**, *12*, 13381–13392. [CrossRef]

87. Güy, N.; Atacan, K.; Özacar, M. Rational Construction of P-n-p CuO/CdS/CoWO_4 S-Scheme Heterojunction with Influential Separation and Directional Transfer of Interfacial Photocarriers for Boosted Photocatalytic H_2 Evolution. *Renew. Energy* **2022**, *195*, 107–120. [CrossRef]

88. Ahmad, I.; Shukrullah, S.; Naz, M.Y.; Bhatti, H.N.; Khalid, N.R.; Ullah, S. Rational Design of ZnO–CuO–Au S-Scheme Heterojunctions for Photocatalytic Hydrogen Production under Visible Light. *Int. J. Hydrogen Energy* **2023**, *48*, 12683–12698. [CrossRef]

89. Subha, N.; Mahalakshmi, M.; Myilsamy, M.; Neppolian, B.; Murugesan, V. Direct Z-Scheme Heterojunction Nanocomposite for the Enhanced Solar H_2 Production. *Appl. Catal. A Gen.* **2018**, *553*, 43–51. [CrossRef]

90. Kannan, K.; Gautam, J.; Chanda, D.; Meshesha, M.M.; Jang, S.G.; Yang, B.L. Two Dimensional MAX Supported Copper Oxide/Nickel Oxide/MAX as an Efficient and Novel Photocatalyst for Hydrogen Evolution. *Int. J. Hydrogen Energy* **2023**, *48*, 7273–7283. [CrossRef]

91. Su, W.N.; Ayele, D.W.; Chen, H.M.; Pan, C.J.; Ochie, V.; Chiang, K.T.; Rick, J.; Hwang, B.J. A Wireless and Redox Mediator-Free Z-Scheme Twin Reactor for the Separate Evolution of Hydrogen and Oxygen. *Mater. Today Energy* **2019**, *12*, 208–214. [CrossRef]

92. Mao, J.X.; Wang, J.C.; Gao, H.; Shi, W.; Jiang, H.P.; Hou, Y.; Li, R.; Zhang, W.; Liu, L. S-Scheme Heterojunction of CuBi$_2$O$_4$ Supported Na Doped P25 for Enhanced Photocatalytic H$_2$ Evolution. *Int. J. Hydrogen Energy* **2022**, *47*, 8214–8223. [CrossRef]

93. Suzuki, K.; Mizuno, N.; Yamaguchi, K. Polyoxometalate Photocatalysis for Liquid-Phase Selective Organic Functional Group Transformations. *ACS Catal.* **2018**, *8*, 10809–10825. [CrossRef]

94. Bharagav, U.; Reddy, N.R.; Rao, V.N.; Ravi, P.; Sathish, M.; Shankar, M.V.; Kumari, M.M. CuWO$_4$ as a Novel Z-Scheme Partner to Construct TiO$_2$ Based Stable and Efficient Heterojunction for Photocatalytic Hydrogen Generation. *Int. J. Hydrogen Energy* **2022**, *47*, 40391–40406. [CrossRef]

95. Bao, X.; Wang, X.; Li, X.; Qin, L.; Han, S.; Kang, S.Z. CuWO$_{4-x}$ Nanoparticles Incorporated Brookite TiO$_2$ Porous Nanospheres: Preparation and Dramatic Photocatalytic Activity for Light Driven H$_2$ Generation. *Mater. Res. Bull.* **2021**, *136*, 111171. [CrossRef]

96. Li, T.; Jin, Z. Rationally Engineered Avtive Sites for Efficient and Durable Hydrogen Production over γ-Graphyne Assembly CuMoO$_4$ S-Scheme Heterojunction. *J. Catal.* **2023**, *417*, 274–285. [CrossRef]

97. Lemoine, P.; Guélou, G.; Raveau, B.; Guilmeau, E. Crystal Structure Classification of Copper-Based Sulfides as a Tool for the Design of Inorganic Functional Materials. *Angew. Chem. Int. Ed.* **2022**, *61*, e202108686. [CrossRef]

98. Sarilmaz, A.; Yanalak, G.; Aslan, E.; Ozel, F.; Patir, I.H.; Ersoz, M. Shape-Controlled Synthesis of Copper Based Multinary Sulfide Catalysts for Enhanced Photocatalytic Hydrogen Evolution. *Renew. Energy* **2021**, *164*, 254–259. [CrossRef]

99. Ranjith, K.S.; Ranjith Kumar, D.; Huh, Y.S.; Han, Y.-K.; Uyar, T.; Rajendra Kumar, R.T. Promotional Effect of Cu$_2$S–ZnS Nanograins as a Shell Layer on ZnO Nanorod Arrays for Boosting Visible Light Photocatalytic H$_2$ Evolution. *J. Phys. Chem. C* **2020**, *124*, 3610–3620. [CrossRef]

100. Wang, G.; Quan, Y.; Yang, K.; Jin, Z. EDA-Assisted Synthesis of Multifunctional Snowflake-Cu$_2$S/CdZnS S-Scheme Heterojunction for Improved the Photocatalytic Hydrogen Evolution. *J. Mater. Sci. Technol.* **2022**, *121*, 28–39. [CrossRef]

101. Shi, J.; Li, S.; Wang, F.; Gao, L.; Li, Y.; Zhang, X.; Lu, J. In Situ Topotactic Formation of 2D/2D Direct Z-Scheme Cu$_2$S/Zn$_{0.67}$Cd$_{0.33}$S in-Plane Intergrowth Nanosheet Heterojunctions for Enhanced Photocatalytic Hydrogen Production. *Dalt. Trans.* **2019**, *48*, 3327–3337. [CrossRef] [PubMed]

102. Shamraiz, U.; Hussain, R.A.; Badshah, A. Fabrication and Applications of Copper Sulfide (CuS) Nanostructures. *J. Solid State Chem.* **2016**, *238*, 25–40. [CrossRef]

103. Mandari, K.K.; Son, N.; Kang, M. CuS/Ag$_2$O Nanoparticles on Ultrathin g-C$_3$N$_4$ Nanosheets to Achieve High Performance Solar Hydrogen Evolution. *J. Colloid Interface Sci.* **2022**, *615*, 740–751. [CrossRef]

104. Liang, H.; Mei, J.; Sun, H.; Cao, L. Enhanced Photocatalytic Hydrogen Evolution of CdS@CuS Core-Shell Nanorods under Visible Light. *Mater. Mater. Sci. Semicond. Process.* **2023**, *153*, 107105. [CrossRef]

105. Liu, X.; Xu, J.; Li, F.; Liu, Z.; Xu, S. Construction S-Scheme of 2D Nanosheets/1D Nanorod Heterojunction with Compact Interface Contact by Electrostatic Self-Assembly for Efficient Photocatalytic Hydrogen Evolution. *Catal. Lett.* **2023**. [CrossRef]

106. Deng, J.; Zhao, Z.Y.; Duan, Z.G. Interfacial Properties of Cu$_7$S$_4$/MnS Heterostructure from First-Principles Calculations. *J. Phys. Chem. Solids* **2019**, *134*, 141–148. [CrossRef]

107. Yuan, Q.; Liu, D.; Zhang, N.; Ye, W.; Ju, H.; Shi, L.; Long, R.; Zhu, J.; Xiong, Y. Noble-Metal-Free Janus-like Structures by Cation Exchange for Z-Scheme Photocatalytic Water Splitting under Broadband Light Irradiation. *Angew. Chem. Int. Ed.* **2017**, *56*, 4206–4210. [CrossRef]

108. Huangfu, Y.; Xie, Z.; Wang, T.; Ding, J.; Chen, Z.; Zhai, Y. Elucidating the Origin of Enhanced Photocatalytic Hydrogen Production on Tuned Cu$_7$S$_4$/CdS Heterostructures. *Chem. An Asian J.* **2022**, *17*, 202200645. [CrossRef]

109. Yang, Y.; Zheng, X.; Song, Y.; Liu, Y.; Wu, D.; Li, J.; Liu, W.; Fu, L.; Shen, Y.; Tian, X. CuInS$_2$-Based Photocatalysts for Photocatalytic Hydrogen Evolution via Water Splitting. *Int. J. Hydrogen Energy* **2023**, *48*, 3791–3806. [CrossRef]

110. Li, X.; Xie, K.; Song, L.; Zhao, M.; Zhang, Z. Enhanced Photocarrier Separation in Hierarchical Graphitic-C$_3$N$_4$-Supported CuInS$_2$ for Noble-Metal-Free Z-Scheme Photocatalytic Water Splitting. *ACS Appl. Mater. Interfaces* **2017**, *9*, 24577–24583. [CrossRef]

111. Zhang, R.; Wang, H.; Li, Y.Y.; Wang, D.; Lin, Y.; Li, Z.; Xie, T. Investigation on the Photocatalytic Hydrogen Evolution Properties of Z-Scheme Au NPs/CuInS$_2$/NCN-CN XComposite Photocatalysts. *ACS Sustain. Chem. Eng.* **2021**, *9*, 7286–7297. [CrossRef]

112. Zhong, Y.; Zi, J.; Wu, F.; Li, Z.; Luan, X.; Gao, F.; Lian, Z. Defect-Mediated Electron Transfer in Pt-CuInS$_2$/CdS Heterostructured Nanocrystals for Enhanced Photocatalytic H$_2$Evolution. *ACS Appl. Nano Mater.* **2022**, *5*, 7704–7713. [CrossRef]

113. Yang, W.; Ma, G.; Fu, Y.; Peng, K.; Yang, H.; Zhan, X.; Yang, W.; Wang, L.; Hou, H. Rationally Designed Ti$_3$C$_2$ MXene@TiO$_2$/CuInS$_2$ Schottky/S-Scheme Integrated Heterojunction for Enhanced Photocatalytic Hydrogen Evolution. *Chem. Eng. J.* **2022**, *429*, 132381. [CrossRef]

114. Chen, F.; Liao, J.Y.; Lu, X.; Xu, Y.Z.; Jiang, X.H.; Tian, M. Constructing an S-Scheme Heterojunction of 2D/2D Cd$_{0.5}$Zn$_{0.5}$S/CuInS$_2$ Nanosheet with Vacancies for Photocatalytic Hydrogen Generation under Visible Light. *Appl. Surf. Sci.* **2023**, *621*, 156721. [CrossRef]

115. Yoshino, S.; Iwase, A.; Ng, Y.H.; Amal, R.; Kudo, A. Z-Schematic Solar Water Splitting Using Fine Particles of H$_2$-Evolving (CuGa)$_{0.5}$ZnS$_2$ Photocatalyst Prepared by a Flux Method with Chloride Salts. *ACS Appl. Energy Mater.* **2020**, *3*, 5684–5692. [CrossRef]

116. Kato, T.; Hakari, Y.; Ikeda, S.; Jia, Q.; Iwase, A.; Kudo, A. Utilization of Metal Sulfide Material of (CuGa)1-XZn$_2$X$_{S2}$ Solid Solution with Visible Light Response in Photocatalytic and Photoelectrochemical Solar Water Splitting Systems. *J. Phys. Chem. Lett.* **2015**, *6*, 1042–1047. [CrossRef]

117. Dhileepan, M.D.; Lakhera, S.K.; Neppolian, B. Interface Engineering of 0D–1D Cu_2NiSnS_4/TiO_2(B) p–n Heterojunction Nanowires for Efficient Photocatalytic Hydrogen Evolution. *Catal. Today* **2023**, *2*, 114006. [CrossRef]

118. Sun, K.; Zhao, X.; Zhang, Y.; Wu, D.; Zhou, X.; Xie, F.; Tang, Z.; Wang, X. Enhanced Photocarrier Separation in Novel Z-Scheme Cu_2ZnSnS_4/Cu_2O Heterojunction for Excellent Photocatalyst Hydrogen Generation. *Mater. Chem. Phys.* **2020**, *251*, 123172. [CrossRef]

119. Manna, G.; Bose, R.; Pradhan, N. Semiconducting and Plasmonic Copper Phosphide Platelets. *Angew. Chem. Int. Ed.* **2013**, *52*, 6762–6766. [CrossRef] [PubMed]

120. De Trizio, L.; Gaspari, R.; Bertoni, G.; Kriegel, I.; Moretti, L.; Scotognella, F.; Maserati, L.; Zhang, Y.; Messina, G.C.; Prato, M.; et al. Cu_3-XP Nanocrystals as a Material Platform for near-Infrared Plasmonics and Cation Exchange Reactions. *Chem. Mater.* **2015**, *27*, 1120–1128. [CrossRef] [PubMed]

121. Peng, X.; Lv, Y.; Fu, L.; Chen, F.; Su, W.; Li, J.; Zhang, Q.; Zhao, S. Photoluminescence Properties of Cuprous Phosphide Prepared through Phosphating Copper with a Native Oxide Layer. *RSC Adv.* **2021**, *11*, 34095–34100. [CrossRef] [PubMed]

122. Paramanik, L.; Sultana, S.; Parida, K. Energy Band Modulation in Cu_xP(X = 3,1/2)/$PbTiO_3$ via Heterogeneous Erection Induced Benign Junction Interface for Enhanced Photocatalytic H_2 Evolution. *Int. J. Hydrogen Energy* **2022**, *47*, 3893–3905. [CrossRef]

123. Shen, R.; Xie, J.; Lu, X.; Chen, X.; Li, X. Bifunctional Cu_3P Decorated G-C_3N_4 Nanosheets as a Highly Active and Robust Visible-Light Photocatalyst for H_2 Production. *ACS Sustain. Chem. Eng.* **2018**, *6*, 4026–4036. [CrossRef]

124. Ioannidi, A.; Petala, A.; Frontistis, Z. Copper Phosphide Promoted $BiVO_4$ photocatalysts for the Degradation of Sulfamethoxazole in Aqueous Media. *J. Environ. Chem. Eng.* **2020**, *8*, 104340. [CrossRef]

125. Rauf, A.; Ma, M.; Kim, S.; Shah, M.S.A.S.; Chung, C.H.; Park, J.H.; Yoo, P.J. Mediator- and Co-Catalyst-Free Direct Z-Scheme Composites of Bi_2WO_6-Cu_3P for Solar-Water Splitting. *Nanoscale* **2018**, *10*, 3026–3036. [CrossRef] [PubMed]

126. Hua, S.; Qu, D.; An, L.; Jiang, W.; Wen, Y.; Wang, X.; Sun, Z. Highly Efficient P-Type Cu_3P/n-Type g-C_3N_4 Photocatalyst through Z-Scheme Charge Transfer Route. *Appl. Catal. B Environ.* **2019**, *240*, 253–261. [CrossRef]

127. Yang, Z.; Shao, L.; Wang, L.; Xia, X.; Liu, Y.; Cheng, S.; Yang, C.; Li, S. Boosted Photogenerated Carriers Separation in Z-Scheme Cu_3P/$ZnIn_2S_4$ Heterojunction Photocatalyst for Highly Efficient H_2 Evolution under Visible Light. *Int. J. Hydrogen Energy* **2020**, *45*, 14334–14346. [CrossRef]

128. Wang, Q.; Xiao, L.; Liu, X.; Sun, X.; Wang, J.; Du, H. Special Z-Scheme Cu_3P/TiO_2 Hetero-Junction for Efficient Photocatalytic Hydrogen Evolution from Water. *J. Alloys Compd.* **2022**, *894*, 162331. [CrossRef]

129. Ge, G.; Yuan, S.; Liu, Q.; Yang, D.; Shi, J.; Lan, X.; Xiao, K. Insight into the Function of Noble-Metal Free Cu_3P Decorated $Zn_{0.5}Cd_{0.5}S$ for Enhanced Photocatalytic Hydrogen Evolution under Visible Light Irradiation– Mechanism for Continuous Increasing Activity. *Appl. Surf. Sci.* **2022**, *597*, 153660. [CrossRef]

130. Yang, Y.; Chen, J.; Liu, C.; Sun, Z.; Qiu, M.; Yan, G.; Gao, F. Dual-Z-Scheme Heterojunction for Facilitating Spacial Charge Transport Toward Ultra-Efficient Photocatalytic H_2 Production. *Sol. RRL* **2021**, *5*, 2100241. [CrossRef]

131. Wang, K.; Xie, H.; Li, Y.; Wang, G.; Jin, Z. Construction of CoP/Cu3P/Ni2P Double S-Scheme Heterojunctions for Improved Photocatalytic Hydrogen Evolution. *J. Phys. Chem. C* **2022**, *126*, 6947–6959. [CrossRef]

132. Li, Z.H.; He, J.X.; Lv, X.H.; Chi, L.F.; Egbo, K.O.; Li, M.D.; Tanaka, T.; Guo, Q.X.; Yu, K.M.; Liu, C.P. Optoelectronic Properties and Ultrafast Carrier Dynamics of Copper Iodide Thin Films. *Nat. Commun.* **2022**, *13*, 6346. [CrossRef]

133. Jin, Z.; Li, H.; Li, J. Efficient Photocatalytic Hydrogen Evolution over Graphdiyne Boosted with a Cobalt Sulfide Formed S-Scheme Heterojunction. *Chin. J. Catal.* **2022**, *43*, 303–315. [CrossRef]

134. Jin, Z.; Li, T.; Zhang, L.; Wang, X.; Wang, G.; Hao, X. Construction of a Tandem S-Scheme GDY/CuI/CdS-R Heterostructure Based on Morphology-Regulated Graphdiyne (g-C: $_NH_{2n-2}$) for Enhanced Photocatalytic Hydrogen Evolution. *J. Mater. Chem. A* **2022**, *10*, 1976–1991. [CrossRef]

135. Jin, Z.; Li, X.; Li, T.; Li, Y. Graphdiyne (C_nH_{2n-2})-Based GDY/CuI/MIL-53(Al) S-Scheme Heterojunction for Efficient Hydrogen Evolution. *Langmuir* **2022**, *38*, 15632–15641. [CrossRef]

136. Yan, T.; Liu, H.; Jin, Z. Graphdiyne Based Ternary GD-CuI-$NiTiO_3$ S-Scheme Heterjunction Photocatalyst for Hydrogen Evolution. *ACS Appl. Mater. Interfaces* **2021**, *13*, 24896–24906. [CrossRef] [PubMed]

137. Su, P.; Liu, H.; Jin, Z. Hierarchical $Co_3(PO_4)_2$/CuI/g-C_nH_{2n-2} S-Scheme Heterojunction for Efficient Photocatalytic Hydrogen Evolution. *Inorg. Chem.* **2021**, *60*, 19402–19413. [CrossRef]

138. Yang, M.; Li, Y.; Jin, Z. In Situ XPS Proved Graphdiyne (C_nH_{2n-2})-Based CoFe LDH/CuI/GD Double S-Scheme Heterojunction Photocatalyst for Hydrogen Evolution. *Sep. Purif. Technol.* **2023**, *311*, 123229. [CrossRef]

139. Li, M.; Wang, J.; Jin, Z. In Situ X-Ray Photoelectron Spectroscopy (XPS) Demonstrated Graphdiyne (g-C_nH_{2n-2}) Based GDY-CuI/NiV-LDH Double S-Scheme Heterojunction for Efficient Photocatalytic Hydrogen Evolution. *Energy Fuels* **2023**, *37*, 5399–5411. [CrossRef]

140. Wang, G.; Quan, Y.; Hao, X.; Guo, X.; Jin, Z. Strong Redox-Capable Graphdiyne-Based Double S-Scheme Heterojunction 10%GC/Mo for Enhanced Photocatalytic Hydrogen Evolution. *J. Environ. Chem. Eng.* **2023**, *11*, 109119. [CrossRef]

141. Wang, Q.; Gao, Q.; Al-Enizi, A.M.; Nafady, A.; Ma, S. Recent Advances in MOF-Based Photocatalysis: Environmental Remediation under Visible Light. *Inorg. Chem. Front.* **2020**, *7*, 300–339. [CrossRef]

142. Cao, Y.; Wang, G.; Liu, H.; Li, Y.; Jin, Z.; Ma, Q. Regular Octahedron Cu-MOFs Modifies $Mn_{0.05}Cd_{0.95}S$ Nanoparticles to Form a S-Scheme Heterojunction for Photocatalytic Hydrogen Evolution. *Int. J. Hydrogen Energy* **2021**, *46*, 7230–7240. [CrossRef]

143. Quan, Y.; Wang, G.; Jin, Z. Tactfully Assembled CuMOF/CdS S-Scheme Heterojunction for High-Performance Photocatalytic H$_2$ Evolution under Visible Light. *ACS Appl. Energy Mater.* **2021**, *4*, 8550–8562. [CrossRef]

144. Sun, S.; Hisatomi, T.; Wang, Q.; Chen, S.; Ma, G.; Liu, J.; Nandy, S.; Minegishi, T.; Katayama, M.; Domen, K. Efficient Redox-Mediator-Free Z-Scheme Water Splitting Employing Oxysulfide Photocatalysts under Visible Light. *ACS Catal.* **2018**, *8*, 1690–1696. [CrossRef]